Ptp4a1	Protein tyrosine phosphatase 4a1	AI172261	1.15	0.010	1.27	0.000	1.35	0.001	1370193	at
Ptpn3	Protein tyrosine phosphatase, non-receptor type 3	AI317821	0.93	0.122	0.77	0.012	0.78	0.029	1389362	at
Ptprr	Protein tyrosine phosphatase, receptor type, R	NM 053594	1.06	0.454	1.20	0.008	1.33	0.000	1368358	a at
Rbx1	Ring-box 1	AI179646	0.83	0.092	1.43	0.012	1.35	0.016	1388538	at
RGD1304758	Similar to RIKEN cDNA 2010008E23 gene	AI412948	1.01	0.976	0.76	0.010	0.79	0.002	1373244	at
RGD1310090	Similar to 2310043K02Rik protein	BI291423	1.04	0.745	0.74	0.009	0.76	0.009	1372359	at
RGD1310450	Similar to hypothetical protein	AI500903	1.06	0.774	1.38	0.035	1.27	0.011	1396842	at
Rnf138	Ring finger protein 138	AW529177	1.23	0.223	1.45	0.009	1.35	0.033	1382379	at
Rock1	Rho-associated coiled-coil forming kinase 1	NM 031098	0.96	0.729	1.76	0.017	1.52	0.002	1368932	at
Rock2	Rho-associated coiled-coil forming kinase 2	NM 013022	0.74	0.042	0.53	0.004	0.69	0.004	1387379	at
Sbf1 predicted	SET binding factor 1 (predicted)	AW434982	0.91	0.493	0.75	0.009	0.79	0.036	1377174	at
Stk3	Serine/threonine kinase 3	NM 031735	0.86	0.010	1.52	0.004	1.22	0.005	1369712	at
Tlk1 predicted	Tousled-like kinase 1 (predicted)	BG379991	1.04	0.496	1.31	0.004	1.31	0.001	1382114	at
Ubadc1	Ubiquitin associated domain containing 1	BI275880	1.06	0.269	0.83	0.030	0.82	0.009	1388387	at
Ube2e	Ubiquitin-conjugating enzyme E2D 2	AW142720	1.03	0.966	1.64	0.008	1.45	0.019	1370523	a at

Regulation of cellular process

Symbol	Description	Accession No.	Sham		OBX + Imipramine		OBX + SNC80		Probe	
			Fold change	*P*-value	Fold change	*P*-value	Fold change	*P*-value		
Adrbk1	Adrenergic receptor kinase, beta 1	NM 012776	0.85	0.149	0.74	0.024	0.83	0.037	1387429	at
Api5 predicted	Apoptosis inhibitor 5 (predicted)	H34636	1.05	0.583	1.57	0.017	1.50	0.002	1395894	at
Bbc3	Bcl-2 binding component 3	AI236152	1.16	0.483	1.60	0.014	1.32	0.015	1382993	at
Bcl2l1	Bcl2-like 1	AF279286	1.08	0.971	0.69	0.041	0.69	0.049	1370485	a at
Btg3	B-cell translocation gene 3	NM 019290	1.37	0.025	1.48	0.020	1.32	0.015	1368072	at
Cacna1a	Calcium channel, voltage-dependent, P/Q type, alpha 1A subunit	AF051527	0.85	0.294	0.64	0.019	0.65	0.031	1386939	a at
Cav2	Caveolin 2	NM 131914	1.07	0.632	1.67	0.013	1.46	0.003	1370135	at
Ccnl2	Cyclin L2	AA892159	0.87	0.236	1.24	0.016	1.21	0.042	1389564	at
Cd38	CD38 antigen	BI289418	1.10	0.009	1.65	0.004	1.34	0.031	1390325	at
Centg3 predicted	Centaurin, gamma 3 (predicted)	AW252124	0.80	0.284	0.62	0.044	0.69	0.022	1376499	at
Chd6 predicted	Chromodomain helicase DNA binding protein 6 (predicted)	BF398050	0.87	0.302	1.37	0.048	1.36	0.025	1379580	at
Cic predicted	Capicua homolog (Drosophila) (predicted)	AI029769	0.98	0.977	0.71	0.003	0.73	0.012	1382322	a at
Cml2	Camello-like 2	NM 021668	1.45	0.087	0.69	0.013	0.59	0.019	1368366	at
Cml3	Camello-like 3	AF187814	1.44	0.061	0.54	0.016	0.49	0.007	1370991	at
Cnot7 predicted	CCR4-NOT transcription complex, subunit 7 (predicted)	BE111850	0.95	0.632	1.23	0.001	1.31	0.003	1367515	at
Crebbp	CREB binding protein	BF566908	0.88	0.245	0.46	0.008	0.73	0.008	1385852	at
Csnk2a2 predicted	Casein kinase II, alpha 2, polypeptide (predicted)	BI290750	1.30	0.021	0.71	0.019	0.82	0.039	1378282	at
Cx3cl1	Chemokine (C-X3-C motif) ligand 1	NM 134455	1.09	0.409	0.68	0.001	0.76	0.011	1368200	at
Dapk3	Death-associated protein kinase 3	AI029121	0.97	0.466	1.41	0.009	1.51	0.043	1383448	at *4
Ddx5	ddx5 gene	AA851926	0.91	0.052	1.31	0.004	1.23	0.027	1371837	at
Dio2	Deiodinase, iodothyronine, type II	NM 031720	1.13	0.215	0.77	0.015	0.81	0.014	1387103	s at *5
Dlc1	Deleted in liver cancer 1	AI176713	0.98	0.251	0.82	0.008	0.81	0.017	1373291	at
Egr1	Early growth response 1	NM 012551	1.19	0.162	0.80	0.035	0.68	0.004	1368321	at
Egr4	Early growth response 4	NM 019137	1.54	0.001	0.78	0.035	0.71	0.011	1387442	at
Fmr1	Fragile X mental retardation syndrome 1 homolog	AI705393	0.93	0.288	1.25	0.047	1.26	0.006	1393459	at
Gabpa predicted	GA repeat binding protein, alpha (predicted)	BG372192	0.85	0.058	1.77	0.001	1.43	0.001	1383377	at
Gnal1	Guanine nucleotide binding protein, alpha 11	NM 031033	0.91	0.060	0.81	0.025	0.80	0.042	1387822	at
Gpsm1	G-protein signalling modulator 1 (AGS3-like, *C. elegans*)	AW435429	1.01	0.191	1.23	0.003	1.21	0.007	1372383	at
Havcr2	Hepatitis A virus cellular receptor 2	BF399036	1.05	0.435	1.43	0.009	1.22	0.011	1377263	at *2
Hdac4 predicted	Histone deacetylase 4 (predicted)	BF419085	0.88	0.107	0.79	0.003	0.74	0.009	1376761	at
Homer1	HS1 binding protein	AB003726	0.79	0.119	0.54	0.001	0.48	0.040	1370454	at
Homer1	HS1 binding protein	AF030088	1.41	0.272	0.46	0.001	0.32	0.004	1370997	at
Hsd3b7	Hydroxy-delta-5-steroid dehydrogenase, 3 beta- and steroid delta-isomerase 7	AB000199	0.91	0.444	1.21	0.019	1.22	0.013	1370433	at
Ift88 predicted	Intraflagellar transport 88 homolog (Chlamydomonas) (predicted)	AI547895	1.01	0.505	1.24	0.012	1.26	0.002	1384915	at
Ighmbp2	Immunoglobulin mu binding protein 2	NM 031586	0.88	0.112	0.79	0.009	0.81	0.048	1368855	at
Ing1	Inhibitor of growth family, member 1	AI170649	0.99	0.020	0.83	0.023	0.83	0.006	1373457	at
Jak3	Janus kinase 3	NM 012855	0.68	0.122	1.89	0.002	1.34	0.017	1368251	at
Kcnh1	Potassium voltage-gated channel, subfamily H (eag-related), member 1	NM 031742	1.06	0.224	0.78	0.002	0.76	0.020	1368061	at
Khsrp	KH-type splicing regulatory protein	BI295086	0.89	0.303	0.57	0.002	0.75	0.043	1375426	a at
Kitl	Kit ligand	BG374178	0.87	0.133	0.76	0.022	0.75	0.004	1388856	at
Limd1 predicted	LIM domains containing 1 (predicted)	BI289676	0.92	0.673	1.46	0.001	1.26	0.020	1372668	at
LOC497729	Hypothetical gene supported by NM 172157	AI412401	0.83	0.047	1.25	0.031	1.37	0.019	1381925	x at
LOC499900	Similar to Zinc finger protein 133	AI146063	1.25	0.076	1.25	0.001	1.41	0.035	1389709	at
Madd	MAP-kinase activating death domain	NM 053585	0.97	0.292	0.77	0.001	0.74	0.013	1369066	at
Mina	Myc induced nuclear antigen	BI278157	0.98	0.973	1.36	0.001	1.22	0.009	1392743	at
Mrps31 predicted	Mitochondrial ribosomal protein S31 (predicted)	AI171229	1.01	0.909	0.83	0.025	0.80	0.010	1372456	at
Mtap2	Microtubule-associated protein 2	X74211	0.91	0.417	0.57	0.009	0.78	0.028	1368411	a at
Mvk	Mevalonate kinase	AW433971	1.01	0.886	0.63	0.029	0.78	0.006	1387119	at
Myt1 predicted	Myelin transcription factor 1 (predicted)	AI070390	1.20	0.331	1.41	0.004	1.53	0.029	1392332	at
Ngfrap1	Nerve growth factor receptor (TNFRSF16) associated protein 1	BG381021	0.89	0.103	1.32	0.018	1.22	0.026	1385534	at
Pacsin1	Protein kinase C and casein kinase substrate in neurons 1	NM 017294	0.92	0.280	0.56	0.006	0.80	0.034	1368958	at
Phf12	PHD finger protein 12	AA924840	1.02	0.818	1.49	0.009	1.49	0.003	1394014	at
Pias4	Protein inhibitor of activated STAT, 4	AI412927	0.96	0.467	0.71	0.007	0.81	0.015	1398352	at
Pik3ca	Phosphatidylinositol 3-kinase, catalytic, alpha polypeptide	AA964375	0.89	0.321	1.55	0.002	1.48	0.001	1393499	at
Prrc1	Proline rich 2	U61729	1.07	0.040	1.44	0.000	1.21	0.046	1370381	at
Pspc1	Paraspeckle protein 1	AI136693	0.96	0.676	1.45	0.011	1.52	0.010	1384465	at
Pycard	PYD and CARD domain containing	BI282953	0.64	0.052	1.77	0.004	1.31	0.044	1389873	at
Rasa1	RAS p21 protein activator 1	BG668164	1.03	0.757	1.57	0.000	1.34	0.010	1393173	at
Rbbp9	Retinoblastoma-binding protein 9	AA956258	0.89	0.206	1.45	0.002	1.35	0.007	1394033	at
Ripk1 predicted	Receptor (TNFRSF)-interacting serine-threonine kinase 1 (predicted)	BF289001	0.80	0.180	1.45	0.012	1.24	0.039	1371529	at
Rock1	Rho-associated coiled-coil forming kinase 1	NM 031098	0.96	0.729	1.76	0.017	1.52	0.002	1368932	at
Runx1t1	Runt-related transcription factor 1; translocated to, 1 (cyclin D-related)	BE105678	0.78	0.006	1.42	0.006	1.55	0.004	1385519	at

Runx1t1	Runt-related transcription factor 1; translocated to, 1 (cyclin D-related)	BF408914	1.05	0.293	0.53	0.029	0.61	0.035	1393901	at
Sbf1 predicted	SET binding factor 1 (predicted)	AW434982	0.91	0.493	0.75	0.009	0.79	0.036	1377174	at
Scap predicted	SREBP cleavage activating protein (predicted)	AI145323	0.98	0.715	1.41	0.030	1.33	0.045	1384464	at
Sec14l2	SEC14-like 2 (*S. cerevisiae*)	AI575603	1.00	0.702	0.75	0.032	0.80	0.026	1374308	at
Sept5	Septin 5	NM 053931	0.99	0.404	0.67	0.009	0.78	0.038	1367852	s at
Sh3md2	Putative scaffolding protein POSH	BG372003	0.98	0.503	1.70	0.033	1.50	0.026	1397620	at
Slc12a4	Solute carrier family 12, member 4	NM 019229	0.77	0.090	2.02	0.006	1.26	0.041	1368125	at
Snx17	Sorting nexin 17	BE329329	0.95	0.292	0.81	0.027	0.82	0.000	1373061	at
Sphk2	Sphingosine kinase 2	AI716502	0.96	0.518	1.54	0.036	1.43	0.027	1376216	at
Stim1 predicted	Stromal interaction molecule 1 (predicted)	BI292282	0.98	0.732	0.70	0.002	0.80	0.011	1382121	at
Stk3	Serine/threonine kinase 3	NM 031735	0.86	0.010	1.52	0.004	1.22	0.005	1369712	at
Taf9l	TAF9-like RNA polymerase II, TATA box binding protein (TBP)-associated factor, 31 kDa	NM 133615	1.03	0.690	1.21	0.036	1.33	0.005	1368429	at
Tcfcp2 predicted	Transcription factor CP2 (predicted)	AW527419	0.96	0.653	1.58	0.000	1.67	0.000	1378218	at
Tgfb2	Transforming growth factor, beta 2	NM 031131	0.91	0.388	1.44	0.007	1.24	0.001	1387172	a at
Thoc1	THO complex 1	BM384228	0.92	0.187	1.22	0.010	1.37	0.016	1376641	at
Tlk1 predicted	Tousled-like kinase 1 (predicted)	BG379991	1.04	0.496	1.31	0.004	1.31	0.001	1382114	at
Tmod1	Tropomodulin 1	AI104913	1.28	0.022	0.73	0.004	0.75	0.004	1388718	at
Txnl1	Thioredoxin-like 1	BF555110	1.04	0.101	1.22	0.005	1.21	0.006	1380191	s at
Ubtf	Upstream binding transcription factor, RNA polymerase I	AI105117	0.99	0.894	0.76	0.001	0.81	0.009	1389830	at
Vipr1	Vasoactive intestinal peptide receptor 1	BI301509	0.94	0.512	0.69	0.035	0.78	0.028	1383695	at
Zfhx1b	Zinc finger homeobox 1b	AW529031	0.84	0.487	1.36	0.016	1.26	0.014	1390940	at
Zfhx1b	Zinc finger homeobox 1b	BG377397	0.79	0.778	1.43	0.005	1.91	0.004	1393795	at *6
Zfp131	Zinc finger protein 131	AA924380	0.99	0.520	1.67	0.008	1.51	0.012	1393780	at
Zfp446 predicted	Zinc finger protein 446 (predicted)	BM389392	1.03	0.569	1.35	0.030	1.22	0.009	1391702	at
Zfp61	Zinc finger protein 61	AI030120	0.90	0.534	1.22	0.012	1.33	0.030	1398663	at
Znf386	Zinc finger protein 386 (Kruppel-like)	NM 019620	0.82	0.066	1.43	0.014	1.25	0.044	1368712	at

Regulation of neurotransmitter levels

Symbol	Description	Accession No.	Sham		OBX + Imipramine		OBX + SNC80		Probe	
			Fold change	*P*-value	Fold change	*P*-value	Fold change	*P*-value		
Glul	Glutamate-ammonia ligase (glutamine synthase)	BM386267	1.00	0.473	0.80	0.038	0.75	0.015	1375569	at
Hnmt	Histamine N-methyltransferase	NM 031044	1.06	0.821	1.32	0.040	1.44	0.004	1387382	at
Sec10l1	Sec10-like 1 (*S. cerevisiae*)	BF386083	1.04	0.790	1.68	0.004	1.42	0.005	1395155	at *7
Sept5	Septin 5	NM 053931	0.99	0.404	0.67	0.009	0.78	0.038	1367852	s at
Slc1a3	Solute carrier family 1 (glial high affinity glutamate transporter), member 3	X63744	0.81	0.449	1.34	0.011	1.43	0.047	1371130	at
Stx1a	Syntaxin 1A (brain)	NM 053788	0.99	0.769	0.71	0.009	0.78	0.038	1387359	at
Syt12	Synaptotagmin XII	AW527241	1.04	0.093	0.67	0.001	0.77	0.018	1398099	at *2
Tgfb2	Transforming growth factor, beta 2	NM 031131	0.91	0.388	1.44	0.007	1.24	0.001	1387172	a at
Unc13c	Unc-13 homolog C (*C. elegans*)	U75361	0.85	0.121	0.71	0.045	0.70	0.017	1370546	at

*1: no symbol, *2: no assignment symbol and description by NetAffx, *3: assign Mageh1 (melanoma antigen, family H, 1) by NetAffx, *4: assign Irf9 (interferon regulatory factor 9) by NetAffx, *5: assign Slc25a14 (solute carrier family 25, member 14) by NetAffx, *6: assign Zeb2 (zinc finger E-box binding homeobox 2) by NetAffx, *7: assign Exoc5 (exocyst complex component 5) by NetAffx.

tion of the genes affected by imipramine and SNC80 treatment. Table 2 lists differentially expressed genes identified according to selected enriched gene ontology terms. Figure 4 showed the systematic scheme of Table 1.

Discussion

In the present study, chronic administration of imipramine or SNC80 significantly reduced hyperemotionality in OBX rats (Fig. 1). The changes of emotional response were consistent with our previous report (21).

On the other hand, we have previously performed several behavioral experiments including the elevated plus maze test in OBX rats (21, 30). OBX rats showed a decrease of the time spent and the number of entries in the open arm of a plus-maze test with vehicle treatment for 7 days, and a recovery of those with treatment of SNC80 and desipramine (21). Thus, the molecular systems affected by imipramine and SNC80 treatment in OBX rats may also be related to antianxiety-like action in addition to antidepressant-like action.

In the frontal cortex, glucose metabolism, blood flow, and electroencephalograph activity are altered in depressed patients (31). Thus, we analyzed frontal cortex samples in this study. However, it is necessary to examine the gene expression profile in the hippocampus and other related brain structures in future.

Gene expression analysis can be used to explain the effects of drugs. Hierarchical cluster analysis can reveal drug action characteristics and thus can be used to estimate the differences and similarities in the actions of various drugs. In the present study, we used gene expression analysis to determine the mechanisms of action of two drugs, imipramine and SNC80, in an animal model of depression. Hierarchical clustering analysis of gene expression data assigned samples from the same drug treatment group into a single cluster (Fig. 2), indicating these samples shared similar gene expression patterns. Indeed, we found that gene expression patterns were similar in OBX rats treated chronically with the antidepressant imipramine and those

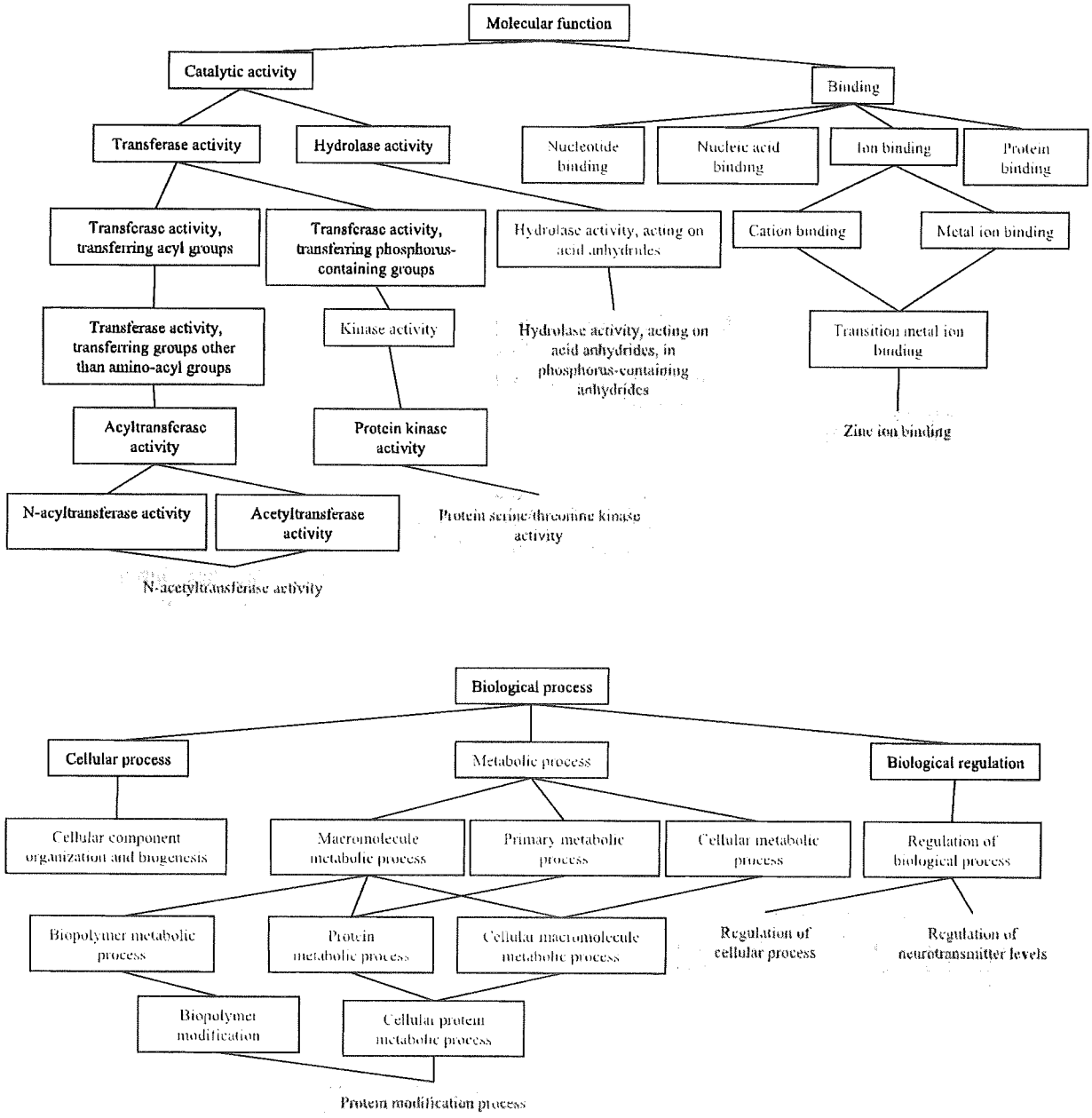

Fig. 4. Functional clustering of the genes affected by imipramine and SNC80 treatment. Biological/functional classifications are organized according to GO pathways, which are linked as hierarchical clusters, with the most general function positioned at a primary node and more specific functions positioned at subsequent nodes. The red characters indicate the functional classifications, which showed statistical significance of association between the 577 genes and GO database ($P<0.01$). Differentially expressed genes identified according to selected enriched gene ontology terms (highlighted in blue) are shown in Table 2.

treated chronically with the delta-opioid agonist SNC80. This is consistent with findings from primary cultures treated in vitro with CNS acting drugs (opioids, antidepressants, and antipsychotic drugs) (32). Microarray analysis of these cells showed that the gene expression profile of cells treated with antidepressants was similar to that of cells treated with a delta-opioid agonist.

The similarity in the effects of imipramine and SNC80 on gene expression was also seen when significant changes in gene expression were analyzed further (Fig. 3). A total of 577 genes were significantly affected by imipramine and SNC80 treatment. Of the 577 genes,

only 3 genes responded oppositely to imipramine and SNC80 treatment (Fig. 3e), suggesting that the CNS functions affected by these drugs were more similar than dissimilar. Interestingly, 35 genes responded to drug treatment by adjusting their expression levels to that of the sham (Fig. 3c). Taken together, our findings indicate that in OBX rats the mechanisms underlying drug action differ from those mediating emotional changes. In the clinical situation, the pathogenic development of depression may be different from the mechanism of antidepressant action.

The elucidation of the mechanisms that direct antidepressant actions should be approached from the viewpoint of the CNS as a whole. One such approach is based on the analysis of a large number of gene expression changes. To date, antidepressants have been reported to affect the expression of many immediate early genes and transcription factors. These regulatory proteins induce many changes in the expression of downstream genes. GeneChip® technology has proven to be very useful for analyzing a large number of genes. However, replicating gene expression data has been problematic. The reproducibility of microarray techniques has been evaluated by way of laboratory correlations and different platform correlations (cDNA microarrays and oligonucleotide chips). These studies showed that gene-by-gene comparisons show exceedingly poor correlation among platforms and across laboratories (33 – 38). However, the reproducibility improved substantially when microarray analysis was based on commonly accepted biological GO terms as opposed to analysis based on gene-by-gene comparisons (35). Consequently, we analyzed mechanisms underlying antidepressant actions based on functional classes rather than on individual gene comparisons. Identifying the functional classes that are affected by antidepressants would lead to the identification of candidate neuronal systems affected by antidepressant treatments. It will be necessary to analyze the individual gene expression changes in future studies.

On the basis of the above analysis schema, we identified common functional changes induced by imipramine and SNC 80 in OBX rats. Using the GO database, we also related the changes we observed in gene expression to specific functions, which included zinc ion binding; hydrolase activity, acting on acid anhydrides, in phosphorus-containing anhydrides; protein serine/threonine kinase activity; N-acetyltransferase activity; protein modification process; regulation of cellular process; and regulation of neurotransmitter levels.

We examined the gene expression analysis at 24 h after the last drug administration to exclude possible acute effects by the drug treatments. However, it is difficult to distinguish antidepressant-like effects from withdrawal effects. In the future, it will be necessary to make clear which functional classes are important for recovery of depressed patients.

Zinc ion binding

During the last several years, important roles of zinc in the psychopathology and therapy of depression have been identified. Recently, clinical data have revealed lower serum zinc concentration in depressed patients (39, 40). Clinical studies have shown zinc supplementation to be beneficial in the antidepressant therapy of depressed patients (41). Zinc also exhibits antidepressant-like effects in behavioral tests and models used to evaluate antidepressant activity, such as the forced swim test and tail suspension test (42 – 44), and in olfactory bulbectomy, chronic mild stress (CMS), and chronic unpredictable stress (CUS) animal models of depression (45 – 47). A recent study demonstrated that acute and chronic treatment with zinc has antidepressant-like effects in OBX rats tested in a passive avoidance task (45). Zinc also significantly decreased the time of walking and number of rearing and peeping in the OBX rats (45). Moreover, chronic zinc treatment reversed the CMS-induced reduction in the consumption of 1% sucrose solution by rats (46). Recently, prolonged zinc treatment has been shown to prevent a deficit in fighting behavior in rats in the CUS model (47). Moreover, in the same model, zinc supplementation potentiated the antidepressant effects of imipramine (47). All of these animal data strongly suggest that zinc possesses possible antidepressant activity.

Hydrolase activity, acting on acid anhydrides, in phosphorus-containing anhydrides

Genes encoding proteins that participate in the hydrolysis of phosphorus-containing acid anhydrides are thought to be involved in various brain functions. Therefore, it is difficult to ascertain the specific action of antidepressants based on this category. However, many genes assigned to this category are related to the ATP-binding cassette (ABC) transporter, which regulates the concentration of drugs in the CNS. Antidepressants are reportedly effluxed from the CNS by the ABC transporter (48, 49). In addition, various antidepressant compounds are differentially recognized as substrates for the ABC transporter (48, 49), and certain substrates such as St. John's wort, a known herbal antidepressant, increase the expression and function of the ABC transporter (50, 51). Indeed, antidepressants may affect ABC transporter activity, thus regulating permeability of the blood brain barrier itself.

Protein serine/threonine kinase activity, protein modification process, and regulation of cellular process

Because genes encoding proteins involved in protein serine/threonine kinase activity, protein modification, or regulation of cellular process have diverse functions, it is difficult to identify the specific actions of antidepressants on the basis of these categories. Each category contained many axonal/dendritic-related genes, N-glycan biosynthesis–related genes, and signal transduction-related genes. However, the present study did not determine the specific function of the genes in the CNS. Further studies are needed.

N-Acetyltransferase activity

A gene that is related to N-acetyltransferase activity has been reported to be involved in antidepressant actions. Serotonin N-acetyltransferase catalyzes the rate-limiting step in the biosynthesis of the circadian hormone melatonin from serotonin. Chronic but not acute fluoxetine administration increases the expression of serotonin N-acetyltransferase in the prefrontal cortex and the hippocampus (52, 53).

This category also contained the Camello protein family and O-GlcNAc transferase protein. Camello proteins, which are localized in the Golgi complex, inhibit gastrulation in *Xenopus laevis*. Camello proteins participate in the acetylation of sugar residues in glycoproteins (54). O-GlcNAc transferase catalyzes the addition of a single N-acetylglucosamine to proteins. Therefore, antidepressants may affect N-acetyltransferase–regulated biosynthesis, especially the modification of glycoproteins.

Regulation of neurotransmitter levels

Antidepressants may regulate neurotransmitter levels, especially glutamate levels, in the synaptic cleft via regulation of exocytosis machinery and uptake machinery. Some clinical studies suggest that the glutamatergic system in depressed patients is pathological. For example, plasma and cerebrospinal fluid glutamate levels and glutamate/glutamine ratios are altered in depressed patients (55 – 57). More recent proton magnetic resonance spectroscopic analyses have identified alterations in glutamate levels in the anterior cingulate cortex and occipital cortex of depressed patients (58, 59). In addition, decreases in glial cell densities observed in depressed patients (60 – 62) may result in decreased glial glutamate transporter expression, thereby reducing the capacity to regulate synaptic concentrations of glutamate. Indeed, one microarray study suggested that glial glutamate transporter expression is decreased in the anterior cingulate cortex and dorsolateral prefrontal cortex of depressed patients (63). Glutamate uptake by glia is the primary mechanism for clearing glutamate from the synaptic cleft. Therefore, a glial deficit may contribute to glutamate hyperactivity in depressed patients.

The inhibition of glutamate release by antidepressant treatment has been reported. Two different drugs (imipramine and phenelzine) were found to reduce depolarization-evoked glutamate overflow from slices of prefrontal cortex after both acute and chronic treatment (64). Acute exposure to fluoxetine reduces depolarization-evoked glutamate release from cerebrocortical synaptosomes in vitro via inhibition of P/Q-type Ca^{2+} channels (65). Chronic antidepressant treatment suppresses depolarization-evoked release of glutamate from hippocampal synaptosomes, by reducing syntaxin-1/CaM kinase II interaction, activity that promotes neurotransmitter release. This treatment also increases syntaxin-1/Munc-18 interaction, an activity that reduces neurotransmitter release (66).

In the present study, we identified an astrocyte-expressed gene that regulates glutamate levels (Glul, Slc1a3). Previously, we also found an astrocyte-expressed gene, Ndrg2, whose expression was decreased by antidepressant treatments in the frontal cortex (67). These results suggest that antidepressants affect not only genes expressed by neurons but also by genes expressed by astrocytes. One of the antidepressant actions may regulate glutamate homeostasis via astrocytes.

Conclusions

In the present study, comprehensive gene expression analyses showed that two drugs with different mechanisms of action affected common neuronal systems in the frontal cortex of OBX rats. Defining the roles of these candidate neuronal systems in antidepressant-induced neural changes is likely to transform the course of research on the biological basis of mood disorders. Such detailed knowledge will have profound effects on the diagnosis, prevention, and treatment of depression.

Acknowledgments

This work was supported in part by Health Science Research Grants from the Japanese Ministry of Health, Labour, and Welfare and the Japanese Ministry of Education, Culture, Sport, Science, and Technology. We thank Dr Keiji Wada and Mr. Naoki Takagaki for the helpful discussions.

References

1 Yamada M, Higuchi T. Functional genomics and depression research. Beyond the monoamine hypothesis. Eur Neuro-

psychopharmacol. 2002;12:235–244.
2 Wong ML, O'Kirwan F, Hannestad JP, Irizarry KJ, Elashoff D, Licinio J. St John's wort and imipramine-induced gene expression profiles identify cellular functions relevant to antidepressant action and novel pharmacogenetic candidates for the phenotype of antidepressant treatment response. Mol Psychiatry. 2004;9: 237–251.
3 Conti B, Maier R, Barr AM, Morale MC, Lu X, Sanna PP, et al. Region-specific transcriptional changes following the three antidepressant treatments electro convulsive therapy, sleep deprivation and fluoxetine. Mol Psychiatry. 2007;12:167–189.
4 Kelly JP, Wrynn AS, Leonard BE. The olfactory bulbectomized rat as a model of depression: an update. Pharmacol Ther. 1997;74:299–316.
5 Song C, Leonard BE. The olfactory bulbectomised rat as a model of depression. Neurosci Biobehav Rev. 2005;29:627–647.
6 Thorne BM, Rowles JS. Memory deficit in passive-avoidance learning in bulbectomized Long-Evans hooded rats. Physiol Behav. 1988;44:339–345.
7 Redmond AM, Kelly JP, Leonard BE. Behavioural and neurochemical effects of dizocilpine in the olfactory bulbectomized rat model of depression. Pharmacol Biochem Behav. 1997;58: 355–359.
8 Okuyama S, Chaki S, Kawashima N, Suzuki Y, Ogawa S, Nakazato A, et al. Receptor binding, behavioral, and electrophysiological profiles of nonpeptide corticotropin-releasing factor subtype 1 receptor antagonists CRA1000 and CRA1001. J Pharmacol Exp Ther. 1999;289:926–935.
9 Ho YJ, Chen KH, Tai MY, Tsai YF. MK-801 suppresses muricidal behavior but not locomotion in olfactory bulbectomized rats: involvement of NMDA receptors. Pharmacol Biochem Behav. 2004;77:641–646.
10 Ho Y, Liu T, Tai M, Wen Z, Chow RS, Tsai Y, et al. Effects of olfactory bulbectomy on NMDA receptor density in the rat brain. Brain Res. 2001;900:214–218.
11 Bilkei-Gorzo A, Racz I, Michel K, Zimmer A. Diminished anxiety- and depression-related behaviors in mice with selective deletion of the Tac1 gene. J Neurosci. 2002;22:10046–10052.
12 Hong KW, Lee WS, Rhim BY. Role of central alpha 2-adrenoceptors on the development of muricidal behavior in olfactory bulbectomized rats: effect of alpha 2-adrenoceptor antagonists. Physiol Behav. 1987;39:535–539.
13 Jesberger JA, Richardson JS. Animal models of depression: parallels and correlates to severe depression in humans. Biol Psychiatry. 1985;20:764–784.
14 Willner P, Mitchell PJ. The validity of animal models of predisposition to depression. Behav Pharmacol. 2002;13:169–188.
15 van Riezen H, Leonard BE. Effects of psychotropic drugs on the behavior and neurochemistry of olfactory bulbectomized rats. Pharmacol Ther. 1990;47:21–34.
16 Cryan JF, McGrath C, Leonard BE, Norman TR. Combining pindolol and paroxetine in an animal model of chronic antidepressant action--can early onset of action be detected? Eur J Pharmacol. 1998;352:23–28.
17 Redmond AM, Kelly JP, Leonard BE. The determination of the optimal dose of milnacipran in the olfactory bulbectomized rat model of depression. Pharmacol Biochem Behav. 1999;62:619–623.
18 Mochizuki D, Tsujita R, Yamada S, Kawasaki K, Otsuka Y, Hashimoto S, et al. Neurochemical and behavioural characterization of milnacipran, a serotonin and noradrenaline reuptake inhibitor in rats. Psychopharmacology (Berl). 2002;162:323–332.
19 Wieronska JM, Papp M, Pilc A. Effects of anxiolytic drugs on some behavioral consequences in olfactory bulbectomized rats. Pol J Pharmacol. 2001;53:517–525.
20 Wieronska JM, Szewczyk B, Branski P, Palucha A, Pilc A. Antidepressant-like effect of MPEP, a potent, selective and systemically active mGlu5 receptor antagonist in the olfactory bulbectomized rats. Amino Acids. 2002;23:213–216.
21 Saitoh A, Yamada M, Yamada M, Takahashi K, Yamaguchi K, Murasawa H, et al. Antidepressant-like effects of the delta-opioid receptor agonist SNC80 ([(+)-4-[(alphaR)-alpha-[(2S,5R)-2,5-dimethyl-4-(2-propenyl)-1-piperazinyl]-(3-methoxyphenyl) methyl]-N,N-diethylbenzamide) in an olfactory bulbectomized rat model. Brain Res. 2008;1208:160–169.
22 Filliol D, Ghozland S, Chluba J, Martin M, Matthes HW, Simonin F, et al. Mice deficient for delta- and mu-opioid receptors exhibit opposing alterations of emotional responses. Nat Genet. 2000;25:195–200.
23 Tejedor-Real P, Mico JA, Smadja C, Maldonado R, Roques BP, Gilbert-Rahola J. Involvement of delta-opioid receptors in the effects induced by endogenous enkephalins on learned helplessness model. Eur J Pharmacol. 1998;354:1–7.
24 Baamonde A, Dauge V, Ruiz-Gayo M, Fulga IG, Turcaud S, Fournie-Zaluski MC, et al. Antidepressant-type effects of endogenous enkephalins protected by systemic RB 101 are mediated by opioid delta and dopamine D1 receptor stimulation. Eur J Pharmacol. 1992;216:157–166.
25 Brady JV, Nauta WJ. Subcortical mechanisms in emotional behavior: the duration of affective changes following septal and habenular lesions in the albino rat. J Comp Physiol Psychol. 1955;48:412–420.
26 Shibata S, Nakanishi H, Watanabe S, Ueki S. Effects of chronic administration of antidepressants on mouse-killing behavior (muricide) in olfactory bulbectomized rats. Pharmacol Biochem Behav. 1984;21:225–230.
27 Yamada M, Iwabuchi T, Takahashi K, Kurahashi C, Ohata H, Honda K, et al. Identification and expression of frizzled-3 protein in rat frontal cortex after antidepressant and electroconvulsive treatment. J Pharmacol Sci. 2005;99:239–246.
28 Hubbell E, Liu WM, Mei R. Robust estimators for expression analysis. Bioinformatics. 2002;18:1585–1592.
29 Dennis G Jr, Sherman BT, Hosack DA, Yang J, Gao W, Lane HC, et al. DAVID: Database for Annotation, Visualization, and Integrated Discovery. Genome Biol. 2003;4:P3.
30 Saitoh A, Yamaguchi K, Tatsumi Y, Murasawa H, Nakatani A, Hirose N, et al. Effects of milnacipran and fluvoxamine on hyperemotional behaviors and the loss of tryptophan hydroxylase-positive cells in olfactory bulbectomized rats. Psychopharmacology (Berl). 2007;191:857–865.
31 Drevets WC, Videen TO, Price JL, Preskorn SH, Carmichael ST, Raichle ME. A functional anatomical study of unipolar depression. J Neurosci. 1992;12:3628–3641.
32 Gunther EC, Stone DJ, Gerwien RW, Bento P, Heyes MP. Prediction of clinical drug efficacy by classification of drug-induced genomic expression profiles in vitro. Proc Natl Acad Sci U S A. 2003;100:9608–9613.
33 Tan PK, Downey TJ, Spitznagel EL Jr, Xu P, Fu D, Dimitrov DS, et al. Evaluation of gene expression measurements from commercial microarray platforms. Nucleic Acids Res. 2003;31: 5676–5684.
34 Yauk CL, Berndt ML, Williams A, Douglas GR. Comprehensive

comparison of six microarray technologies. Nucleic Acids Res. 2004;32:e124.
35 Bammler T, Beyer RP, Bhattacharya S, Boorman GA, Boyles A, Bradford BU, et al. Standardizing global gene expression analysis between laboratories and across platforms. Nat Methods. 2005;2:351–356.
36 Irizarry RA, Warren D, Spencer F, Kim IF, Biswal S, Frank BC, et al. Multiple-laboratory comparison of microarray platforms. Nat Methods. 2005;2:345–350.
37 Larkin JE, Frank BC, Gavras H, Sultana R, Quackenbush J. Independence and reproducibility across microarray platforms. Nat Methods. 2005;2:337–344.
38 Sherlock G. Of fish and chips. Nat Methods. 2005;2:329–330.
39 Maes M, De Vos N, Demedts P, Wauters A, Neels H. Lower serum zinc in major depression in relation to changes in serum acute phase proteins. J Affect Disord. 1999;56:189–194.
40 Maes M, Vandoolaeghe E, Neels H, Demedts P, Wauters A, Meltzer HY, et al. Lower serum zinc in major depression is a sensitive marker of treatment resistance and of the immune /inflammatory response in that illness. Biol Psychiatry. 1997;42:349–358.
41 Nowak G, Siwek M, Dudek D, Zieba A, Pilc A. Effect of zinc supplementation on antidepressant therapy in unipolar depression: a preliminary placebo-controlled study. Pol J Pharmacol. 2003;55:1143–1147.
42 Kroczka B, Branski P, Palucha A, Pilc A, Nowak G. Antidepressant-like properties of zinc in rodent forced swim test. Brain Res Bull. 2001;55:297–300.
43 Szewczyk B, Branski P, Wieronska JM, Palucha A, Pilc A, Nowak G. Interaction of zinc with antidepressants in the forced swimming test in mice. Pol J Pharmacol. 2002;54:681–685.
44 Rosa AO, Lin J, Calixto JB, Santos AR, Rodrigues AL. Involvement of NMDA receptors and L-arginine-nitric oxide pathway in the antidepressant-like effects of zinc in mice. Behav Brain Res. 2003;144:87–93.
45 Nowak G, Szewczyk B, Wieronska JM, Branski P, Palucha A, Pilc A, et al. Antidepressant-like effects of acute and chronic treatment with zinc in forced swim test and olfactory bulbectomy model in rats. Brain Res Bull. 2003;61:159–164.
46 Nowak G, Szewczyk B, Pilc A. Zinc and depression. An update. Pharmacol Rep. 2005;57:713–718.
47 Cieslik K, Klenk-Majewska B, Danilczuk Z, Wrobel A, Lupina T, Ossowska G. Influence of zinc supplementation on imipramine effect in a chronic unpredictable stress (CUS) model in rats. Pharmacol Rep. 2007;59:46–52.
48 Uhr M, Grauer MT, Holsboer F. Differential enhancement of antidepressant penetration into the brain in mice with abcb1ab (mdr1ab) P-glycoprotein gene disruption. Biol Psychiatry. 2003;54:840–846.
49 Uhr M, Steckler T, Yassouridis A, Holsboer F. Penetration of amitriptyline, but not of fluoxetine, into brain is enhanced in mice with blood-brain barrier deficiency due to mdr1a P-glycoprotein gene disruption. Neuropsychopharmacology. 2000; 22:380–387.
50 Seelig A. A general pattern for substrate recognition by P-glycoprotein. Eur J Biochem. 1998;251:252–261.
51 Hennessy M, Kelleher D, Spiers JP, Barry M, Kavanagh P, Back D, et al. St Johns wort increases expression of P-glycoprotein: implications for drug interactions. Br J Clin Pharmacol. 2002;53:75–82.
52 Uz T, Ahmed R, Akhisaroglu M, Kurtuncu M, Imbesi M, Dirim Arslan A, et al. Effect of fluoxetine and cocaine on the expression of clock genes in the mouse hippocampus and striatum. Neuroscience. 2005;134:1309–1316.
53 Uz T, Manev H. Chronic fluoxetine administration increases the serotonin N-acetyltransferase messenger RNA content in rat hippocampus. Biol Psychiatry. 1999;45:175–179.
54 Popsueva AE, Luchinskaya NN, Ludwig AV, Zinovjeva OY, Poteryaev DA, Feigelman MM, et al. Overexpression of camello, a member of a novel protein family, reduces blastomere adhesion and inhibits gastrulation in Xenopus laevis. Dev Biol. 2001;234:483–496.
55 Kim JS, Schmid-Burgk W, Claus D, Kornhuber HH. Increased serum glutamate in depressed patients. Arch Psychiatr Nervenkr. 1982;232:299–304.
56 Altamura C, Maes M, Dai J, Meltzer HY. Plasma concentrations of excitatory amino acids, serine, glycine, taurine and histidine in major depression. Eur Neuropsychopharmacol. 1995;5 Suppl: 71–75.
57 Levine J, Panchalingam K, Rapoport A, Gershon S, McClure RJ, Pettegrew JW. Increased cerebrospinal fluid glutamine levels in depressed patients. Biol Psychiatry. 2000;47:586–593.
58 Auer DP, Putz B, Kraft E, Lipinski B, Schill J, Holsboer F. Reduced glutamate in the anterior cingulate cortex in depression: an in vivo proton magnetic resonance spectroscopy study. Biol Psychiatry. 2000;47:305–313.
59 Sanacora G, Gueorguieva R, Epperson CN, Wu YT, Appel M, Rothman DL, et al. Subtype-specific alterations of gamma-aminobutyric acid and glutamate in patients with major depression. Arch Gen Psychiatry. 2004;61:705–713.
60 Ongur D, Drevets WC, Price JL. Glial reduction in the subgenual prefrontal cortex in mood disorders. Proc Natl Acad Sci U S A. 1998;95:13290–13295.
61 Rajkowska G, Miguel-Hidalgo JJ, Wei J, Dilley G, Pittman SD, Meltzer HY, et al. Morphometric evidence for neuronal and glial prefrontal cell pathology in major depression. Biol Psychiatry. 1999;45:1085–1098.
62 Cotter D, Mackay D, Landau S, Kerwin R, Everall I. Reduced glial cell density and neuronal size in the anterior cingulate cortex in major depressive disorder. Arch Gen Psychiatry. 2001;58:545–553.
63 Choudary PV, Molnar M, Evans SJ, Tomita H, Li JZ, Vawter MP, et al. Altered cortical glutamatergic and GABAergic signal transmission with glial involvement in depression. Proc Natl Acad Sci U S A. 2005;102:15653–15658.
64 Michael-Titus AT, Bains S, Jeetle J, Whelpton R. Imipramine and phenelzine decrease glutamate overflow in the prefrontal cortex – a possible mechanism of neuroprotection in major depression? Neuroscience. 2000;100:681–684.
65 Wang SJ, Su CF, Kuo YH. Fluoxetine depresses glutamate exocytosis in the rat cerebrocortical nerve terminals (synaptosomes) via inhibition of P/Q-type Ca2+ channels. Synapse. 2003;48:170–177.
66 Bonanno G, Giambelli R, Raiteri L, Tiraboschi E, Zappettini S, Musazzi L, et al. Chronic antidepressants reduce depolarization-evoked glutamate release and protein interactions favoring formation of SNARE complex in hippocampus. J Neurosci. 2005;25:3270–3279.
67 Takahashi K, Yamada M, Ohata H, Momose K, Higuchi T, Honda K. Expression of Ndrg2 in the rat frontal cortex after antidepressant and electroconvulsive treatment. Int J Neuropsychopharmacol. 2005;8:381–389.

Behavioral and Brain Functions

BioMed Central

Research

Open Access

The *Frizzled 3* gene is associated with methamphetamine psychosis in the Japanese population

Makiko Kishimoto[1], Hiroshi Ujike*[1,2], Yuko Okahisa[1], Tatsuya Kotaka[1], Manabu Takaki[1], Masafumi Kodama[1], Toshiya Inada[2,3], Mitsuhiko Yamada[2,4], Naohisa Uchimura[2,5], Nakao Iwata[2,6], Ichiro Sora[2,7], Masaomi Iyo[2,8], Norio Ozaki[2,9] and Shigetoshi Kuroda[1]

Address: [1]Department of Neuropsychiatry, Okayama University Graduate School of Medicine, Dentistry and Pharmaceutical Sciences, Okayama, Japan, [2]JGIDA (Japanese Genetics Initiative for Drug Abuse), Japan, [3]Institute of Neuropsychiatry, Seiwa Hospital, Tokyo, Japan, [4]Department of Psychogeriatrics, National Institute of Mental Health, National Center of Neurology and Psychiatry, Kodaira, Japan, [5]Department of Neuropsychiatry, Kurume University Graduate School of Medicine, Kurume, Japan, [6]Department of Psychiatry, Fujita Health University School of Medicine, Houmei, Japan, [7]Department of Neuroscience, Division of Psychobiology, Tohoku University Graduate School of Medicine, Sendai, Japan, [8]Department of Psychiatry, Chiba University Graduate School of Medicine, Chiba, Japan and [9]Department of Psychiatry, Nagoya University Graduate School of Medicine, Nagoya, Japan

Email: Makiko Kishimoto - makiko.kishimoto@nifty.com; Hiroshi Ujike* - hujike@cc.okayama-u.ac.jp; Yuko Okahisa - gmd15031@cc.okayama-u.ac.jp; Tatsuya Kotaka - tatsuya7kotaka7@yahoo.co.jp; Manabu Takaki - manabuta@cc.okayama-u.ac.jp; Masafumi Kodama - m-kodama@cc.okayama-u.ac.jp; Toshiya Inada - han91010@rio.odn.ne.jp; Mitsuhiko Yamada - mitsu@ncnp.go.jp; Naohisa Uchimura - naohisa@med.kurume-u.ac.jp; Nakao Iwata - nakao@fujita-hu.ac.jp; Ichiro Sora - isora@mail.tains.tohoku.ac.jp; Masaomi Iyo - iyom@faculty.chiba-u.jp; Norio Ozaki - ozaki-n@med.nagoya-u.ac.jp; Shigetoshi Kuroda - skuroda@cc.okayama-u.ac.jp

* Corresponding author

Published: 15 August 2008

Behavioral and Brain Functions 2008, 4:37 doi:10.1186/1744-9081-4-37

Received: 5 August 2008
Accepted: 15 August 2008

This article is available from: http://www.behavioralandbrainfunctions.com/content/4/1/37

Abstract

Background: Frizzled 3 (Fzd3) is a receptor required for the Wnt-signaling pathway, which has been implicated in the development of the central nervous system, including synaptogenesis and structural plasticity. We previously found a significant association between the *FZD3* gene and susceptibility to schizophrenia, but subsequent studies showed inconsistent findings. To understand the roles of the *FZD3* gene in psychotic disorders further, it should be useful to examine *FZD3* in patients with methamphetamine psychosis because the clinical features of methamphetamine psychosis are similar to those of schizophrenia.

Methods: Six SNPs of *FZD3*, rs3757888 in the 3' flanking region, rs960914 in the intron 3, rs2241802, a synonymous SNP in the exon5, rs2323019 and rs352203 in the intron 5, and rs880481 in the intron 7, were selected based on the previous schizophrenic studies and analyzed in 188 patients with methamphetamine psychosis and 240 age- and gender-matched controls.

Results: A case-control association analyses revealed that two kinds of *FZD3* haplotypes showed strong associations with methamphetamine psychosis ($p < 0.00001$). Having the G-A-T-G or A-G-C-A haplotype of rs2241802-rs2323019-rs352203-rs880481 was a potent negative risk factor (odds ratios were 0.13 and 0.086, respectively) for methamphetamine psychosis.

Conclusion: Our present and previous findings indicate that genetic variants of the *FZD3* gene affect susceptibility to two analogous but distinct dopamine-related psychoses, endogenous and substance-induced psychosis.

Background

The neurodevelopmental hypothesis of schizophrenia suggests that interaction between genetic and environmental events occurring during critical early periods of neuronal growth may negatively influence the way by which nerve cells are laid down, differentiated, selectively culled by apoptosis and remodeled by expansion and retraction of dendrites and synaptic connections [1,2]. The Wnt family molecules play several roles in neuronal development by inducing cells to proliferate, differentiate, and survive [3,4]. In particular, Wnt signaling plays roles in regulating patterning during cortical development, axon remodeling, synaptic differentiation, clustering of synapsin I at presynaptic terminals [5-7] and the cytoarchitectural derangement that was observed in the brains of schizophrenics [8]. A mutation in the Wnt1 gene, one of the Wnt family genes, leads to abnormal cerebral development in mice [9], and mice deficient in Frizzled 3 (Fzd3), a receptor of Wnt ligands, showed loss of thalamo-cortical tracts and defects in corpus callosum development, abnormalities which were reported in schizophrenic patients [10-12]. Therefore, alteration of the Wnt/Fzd cascade may represent an aberrant neurodevelopment involved in schizophrenia [13].

Fzd3 is a required receptor in the Wnt-signaling pathway. In 2003, we reported a significant association between the gene encoding Fzd3 (*FZD3*) and susceptibility to schizophrenia [14]. Subsequent studies tried to replicate our findings, but the results were inconsistent. Yang et al. [15] revealed a significant association of the *FZD3* gene with schizophrenia in Han Chinese populations by a transmission disequilibrium test, and Zhang et al. [16] also found a significant association by a family-based case-control study. On the other hand, several studies failed to find significant evidence of a genetic effect of the *FZD3* gene on schizophrenia [17-19]. The inconsistencies in genetic studies in the relationship of the *FZD3* gene with schizophrenia may suggest heterogeneity of schizophrenia and a requirement for further studies using larger sample size. We consider that it may be also useful to investigate the role of the *FZD3* gene in other types of psychotic disorders for better understanding of the physiological roles of Fzd3 and the Wnt cascade in schizophrenia or psychotic conditions.

Repeated abuse of methamphetamine frequently predisposes to psychotic conditions. The clinical similarity between methamphetamine psychosis and schizophrenia has been pointed out, and methamphetamine psychosis has been considered to be a pharmacological model of schizophrenia, especially the paranoid subtype [20-22]. Thus, methamphetamine psychosis and schizophrenia resemble each other in a cross-section of clinical features, e.g., auditory hallucination and delusion, the longitudinal process of progressive exacerbation with acute relapses, good response to neuroleptics, and enduring vulnerability to relapse under stressors. Enhanced dopamine release in the striatum due to a challenge dose of methamphetamine was observed in schizophrenic patients and methamphetamine-sensitized rats, an animal model of methamphetamine psychosis [23-25]. These similarities between schizophrenia and methamphetamine psychosis in both symptomatology and pharmacological aspects may suggest that shared neural mechanisms are involved in both psychotic disorders. Therefore, in order to examine the roles of Fzd3 in mechanisms underlying the development of psychosis, we analyzed the *FZD3* gene in patients with methamphetamine psychosis.

Methods

Subjects

The subjects consisted of 188 patients with methamphetamine psychosis (158 male, 30 female; mean age ± SD, 36.6 ± 11.8) and 240 age-, gender-, and geographical origin-matched healthy controls (192 male, 48 female; mean age ± SD, 36.6 ± 10.6), who have no individual or family history of drug dependence or major psychotic disorders such as schizophrenia and bipolar disorders. All the subjects were unrelated Japanese, born and living in relatively restricted areas of Japan, northern Kyushu, Setouchi, Chukyo, Tokai, and Kanto. All subjects were out-patients or inpatients in psychiatric hospitals of the Japanese Genetics Initiative for Drug Abuse (JGIDA), a multicenter collaborative study group. Consensus diagnoses of methamphetamine psychosis were made by two trained psychiatrists according to the ICD-10 criteria on the basis of interviews and medical records. The patients with methamphetamine psychosis in the present study usually showed predominant positive symptoms such as delusion and hallucination. We excluded cases in which the predominant symptoms were of the negative and/or disorganized type in order to maintain the homogeneity of the patient group. The study protocol and purpose were explained to all subjects participating in the study, and written informed consent was obtained from all subjects. This study was approved by the Ethics Committee of each participating institute of JGIDA.

DNA analysis

We genotyped the three single nucleotide polymorphisms (SNPs), rs3757888 (SNP1) in the 3' flanking region, rs960914 (SNP2) in the intron 3, and rs2241802 (SNP3), a synonymous SNP in the exon5 of the *FZD3* gene that were analyzed in our previous study [14]. We also analyzed three additional SNPs, rs2323019 (SNP4) and rs352203 (SNP5) in the intron 5, and rs880481 (SNP6) in the intron 7 of the gene because a significant association with schizophrenia was reported by Yang et al. [15] and Zhang et al. [16]. Genotyping was performed by the PCR-

RFLP method. The genomic DNA was extracted from peripheral leukocytes using phenol-chloroform. Each polymorphic site was amplified by PCR (PCR primer sequence of each SNP is available on request) in a 15-μl volume containing 3% dimethyl sulfoxide and 0.75 units of Taq DNA polymerase (Promega Co., Japan) using a unique primer set. PCR reaction was performed under the following conditions: 95°C for 5 min, then 35 cycles of 30 s of denaturing at 95°C, 1 min of annealing at the appropriate temperature, and 30 s of extension, and final elongation at 72°C for 10 min. The PCR products were digested with the corresponding restriction enzyme for each polymorphism, Dde*I* for rs3757888, Rsa*I* for rs960914, Alu*I* for rs2241802, Ssp*I* for rs2323019, Nla*III* for rs352203, Eco32*I* for rs880481, and then electrophoresed on 3.0% agarose gels and stained with GelStar (TaKaRa Co., Japan). All genotyping was performed in a blinded fashion, with the control and cases samples mixed randomly. The genotyping of the SNPs were confirmed in part by direct sequencing or a TaqMan SNP genotyping assay (Applied Biosystems, Foster City, CA, U.SA.).

Statistical analysis

Statistical analysis of association was performed using SNPAlyze software (Dynacom Co., Japan). Deviation from Hardy-Weinberg equilibrium and case- control study were tested using the χ^2 test for goodness of fit and χ^2 test for dependence, respectively. Linkage disequilibrium (LD) was tested using the χ^2 test, and D' and r^2 values were made the index in the authorization of LD. Case-control haplotype analysis was performed by the permutation method, and permutation *p*-values were calculated based on 100,000 replications.

Results

The genotype distribution and allele frequencies of the each polymorphism are shown in Table 1. The genotype distributions of patients and control subjects did not deviate from Hardy-Weinberg equilibrium at any SNP examined. The allele frequencies of SNP1, SNP2, and SNP3

Table 1: Genotype and allele distribution of six SNPs of the FZD3 gene in controls and patients with methamphetamine (MAP) psychosis

			Genotype			*p*	Allele		*p*
SNP1	rs3757888	N	A/A	A/G	G/G		A	G	
Control		230	198(86.1)	31(13.5)	1(0.4)		427(92.8)	33(7.2)	
MAP Psychosis		186	151(81.2)	32(7.2)	3(1.61)	0.26	334(89.8)	38(10.2)	0.19
SNP2	rs960914	N	T/T	T/C	C/C		T	C	
Control		240	67(27.9)	130(54.2)	43(17.9)		264(55.0)	216(45.0)	
MAP Psychosis		185	45(24.3)	103(55.7)	37(20.0)	0.66	193(52.2)	177(47.8)	0.41
SNP3	rs2241802	N	A/A	A/G	G/G		A	G	
Control		240	49(20.4)	124(51.7)	67(27.9)		222(46.2)	258(53.8)	
MAP Psychosis		181	44(24.3)	97(53.6)	40(22.1)	0.34	185(51.1)	177(48.9)	0.16
SNP4	rs2323019	N	A/A	A/G	G/G		A	G	
Control		239	72(31.4)	113(49.3)	44(19.2)		257(56.1)	201(43.9)	
MAP Psychosis		186	45(24.1)	101(54.0)	41(21.9)	0.25	191((51.1)	183(48.9)	0.15
SNP5	rs352203	N	T/T	T/C	C/C		T	C	
Control		192	64(33.3)	98(51.1)	30(15.6)		226(58.9)	158(41.1)	
MAP Psychosis		176	49(27.8)	98(55.7)	29(16.5)	0.52	196(55.7)	156(44.3)	0.38
SNP6	rs880481	N	A/A	A/G	G/G		A	G	
Control		236	43(18.2)	123(52.1)	70(29.7)		209(44.3)	263(55.7)	
MAP Psychosis		186	30(16.1)	103(55.4)	53(28.5)	0.97	163(43.8)	209(56.2)	0.99

SNP, Single nucleotide polymorphism.
Numbers in parentheses indicate percentages.

were approximately same as those of our previous study [14]. The allele frequencies of SNP4, SNP5, and SNP6 in the present study also showed values similar to those of previous studies of Japanese and Chinese populations [16-18].

We found no significant difference between patients and controls in the frequencies of the genotype or allele at any single SNP of the *FZD3* gene. We estimated the pairwise LD between the six SNPs of the *FZD3* gene using the D' and r^2values as an index (Table 2). A D' range of 0.7–0.9 and a $r^2 > 0.3$ were found between SNP2, SNP3, SNP4, SNP5, and SNP6, but not between SNP1 and the other SNPs. This suggests that SNP2, SNP3, SNP4, SNP5, and SNP6 are in linkage disequilibrium and located within one LD block. Then, we performed case-control haplotype analysis using SNP2 to SNP6 (Table 3). Haplotype analyses revealed significant differences in patients and control subjects at SNP5-6, SNP4-5-6, SNP3-4-5-6, and SNP2-3-4-5-6, but not at SNP2-3, SNP3-4, SNP4-5, SNP2-3-4, SNP3-4-5, or SNP2-3-4-5. The largest χ^2 and smallest permutation *P* values were found in the haplotype analysis of SNP3-4-5-6 ($\chi^2 = 64.8$, permutation $p < 0.00001$). The estimated individual haplotypic frequencies of SNP3-4-5-6 are shown in Table 4. Eight kinds of haplotypes consisting of SNP3-4-5-6 with more than 1% overall frequency were identified. The estimated haplotype frequency of G-A-T-G and A-G-C-A of SNP3-4-5-6 were significantly lower in patients with methamphetamine psychosis than in controls ($p < 0.00001$ and $p = 0.0003$, respectively). Conversely, the A-G-C-G haplotype was significantly in excess in patients compared with controls ($p = 0.0246$). To avoid a type I error due to multiple comparison, Bonferroni's correction was applied to the results. G-A-T-G and A-G-C-A haplotypes were still significantly less frequent in the methamphetamine patients than in the controls, but A-G-C-G was not significantly different between the groups after correction. The odds ratios G-A-T-G and A-G-C-A haplotypes were 0.13 (95%CI; 0.043–0.36) and 0.086 (95%CI; 0.011–0.67), respectively. Accordingly, G-A-T-G and A-G-C-A haplotypes of SNP3-4-5-6 were negative risk haplotypes for methamphetamine psychosis.

Table 2: Pairwise Linkage Disequilibrium between six SNPs of the FZD3 gene

	SNP1	SNP2	SNP3	SNP4	SNP5	SNP6
SNP1		**0.840**	0.557	0.379	**0.853**	**0.706**
SNP2	0.057		**0.760**	**0.915**	**0.970**	**0.749**
SNP3	0.031	**0.532**		**0.834**	**0.831**	**0.729**
SNP4	0.012	**0.829**	**0.627**		**0.982**	**0.760**
SNP5	0.052	**0.841**	**0.542**	**0.843**		**0.788**
SNP6	0.036	**0.377**	**0.389**	**0.387**	**0.367**	

Linkage disequilibrium was tested using χ^2 test. Upper right and lower left diagonals show D' and r-square values, respectively. D'>0.7 and r-square>0.3 were shown in bold.

Discussion

We revealed that the *FZD3* gene is significantly associated with the vulnerability to psychosis induced by methamphetamine abuse, and two haplotypes of the *FZD3* gene comprising SNP3-4-5-6 (rs2241802-rs2323019-rs352203-rs880481) were identified as potent negative risk factors for methamphetamine psychosis. The G-A-T-G and A-G-C-A haplotypes potently reduce the risks of predisposition to psychosis after methamphetamine abuse to one seventh to one eleventh. In our previous study of schizophrenia [14], distribution of the SNP2 genotypes and haplotypes comprising SNP2-SNP3 was significantly associated with schizophrenia. Zhang et al. [16] reported that the haplotype comprising SNP4-SNP5-SNP6 was associated with schizophrenia in a Chinese population. These findings indicate that genetic variants of the *FZD3* gene may affect susceptibility to two analogous but distinct psychoses, endogenous psychosis of schizophrenia and substance-induced psychosis. This may imply that Fzd3 is involved in a liability to psychotic symptoms such as hallucination and delusion irrespective of whether they are due to schizophrenia or methamphetamine psychosis.

Dopamine is a key molecule in the pathophysiology of both schizophrenia and methamphetamine psychosis. Enhanced dopamine release in the terminals of mesolimbic dopamine projections was demonstrated *in vivo* in patients with schizophrenia, and the amount of the increase in dopamine was positively associated with the emergence or worsening of psychotic symptoms [25]. Similar phenomena were demonstrated in mesolimbic and mesocortical terminals in animal models of methamphetamine psychosis [23]. Wnt1 was found to be expressed in close vicinity to developing midbrain dopamine neurons, which are the origins of the mesolimbic and mesocortical dopamine pathways. Wnt1 regulates the genetic network leading to establishment of the midbrain progenitor domain in the ventral midbrain during embryonic development and of the subsequent terminal differentiation of midbrain dopamine neurons [26,27]. It is possible that differences in Wnt signaling due to genetic variants of the *FZD3* gene affect the development of dopamine neurons of the mesolimbic or mesocortical pathway in early brain development and susceptibility to these two dopamine-related psychoses in adulthood.

Another molecule that potentially links Fzd3 and these two related psychoses is glycogen synthesis kinase-3 (GSK-3), a serine/threonine kinase that is a downstream component of the Wnt/Fzd cascades. Binding of Wnt ligands to Fzd family receptors leads to activation of the intracellular protein disheveled, which inactivates GSK-

Table 3: Haplotype analysis of the FZD3 gene

	1SNP	2SNP	3SNP	4SNP	5SNP
SNP ID			Permutation p-value		
SNP2 (rs960914T>C)	0.41	0.16			
SNP3 (rs2241802G>A)	0.16	0.15	0.22	0.35	
SNP4 (rs2323019A>G)	0.15	0.072	0.15	**<0.00001**	**<0.00001**
SNP5 (rs352203T>C)	0.38	**0.00002**	**0.00001**		
SNP6 (rs880481A>G)	0.99				

Haplotype analysis was performed by permutaion method. Bold values represent significant p values.

3β. This in turn leads to the stabilization and accumulation of β-catenin, which translocates to the nucleus where it interacts with nuclear transcription factors for the genes involved in neuronal development. Briefly, GSK-3β mediates Wnt/Fzd signaling cascades. Dysregulation of GSK-3β and 3α is one of promising neurodevelopmental hypotheses of schizophrenia [13,28]. GSK-3 is also regulated by dopamine signaling through protein kinase B [29]. Several studies showed, but not consistently, that GSK-3 protein levels and activities are altered in schizophrenic brains [30,31] and lymphocytes [32,33]. Several genes, e.g., *DISC1* and *NRG1*, which have been repeatedly shown to be associated with susceptibility to schizophrenia, are involved in GSK-3/Wnt regulatory pathways [28]. Recently, the gene encoding DKK4, a component of the GSK-3/Wnt signaling cascade, was shown to be associated with schizophrenia. DKK4 inhibits Wnt-Fzd binding, resulting in inactivation of GSK-3 [34]. On the other hand, amphetamine also affects GSK-3 activity. Administration of amphetamine to mice increased Ser9 phosphorylation of GSK-3β, resulting in a reduction of its activity in the frontal cortex and striatum [35], and GSK-3 gene knockdown mice showed a reduced response to amphetamine [36]. Intriguingly, psychotomimetics of two different classes, phencyclidine and D-lysergic acid, also had the same effects on GSK-3β, which may imply that substance-induced psychosis might be the result of a reduction in GSK-3 signaling. In contrast, chronic treatment with typical and atypical neuroleptics that ameliorate the psychotic symptoms of schizophrenia and methamphetamine psychosis increase the levels and activities of GSK-3 [37]. It was also found that chronic neuroleptic treatment increased β-catenin in the ventral midbrain, whereas amphetamine decreased it [38]. These findings indicate that the altered GSK-3/Wnt signaling is involved in liability to expression of positive psychotic symptoms such as the hallucinations and delusions in patients suffering from both schizophrenia and methamphetamine-induced psychosis. This hypothesis may be supported by our present and previous findings because the *FZD3* gene was significantly associated with not only schizophrenia but also methamphetamine psychosis.

The present results were still significant even after a Bonferroni correction, although it is possibly a chance finding due to less power. The power analysis showed that our

Table 4: Haplotype frequencies from positive permutation analyses

Haplotype	Frequency		Permutation p-values	Odds ratio (95%CI)
(SNP3-4-5-6)	Controls	MAP Psychosis		
G-A-T-A	0.3523	0.4148	0.0889	
A-G-C-G	0.3178	0.3970	0.0246	1.42 (1.14–1.76)
G-A-T-G	0.1542	0.0243	<0.00001	0.13 (0.07–0.22)
A-A-T-G	0.0382	0.0635	0.1283	
A-G-C-A	0.0625	0.0070	0.0003	0.086 (0.03–0.24)
A-G-T-G	0.0211	0.0354	0.2791	
G-G-C-G	0.0196	0.0379	0.1678	
A-A-T-A	0.0169	0.0090	0.4565	

Haplotypes with overall frequencies are less than 1% were eliminated.

present sample size had more than 80% power to detect a significant difference at 0.05 of any SNP examined, but it must have less power for haplotype analyses. Therefore, our findings should be confirmed in studies using a larger number of subjects and different populations. It may also be useful for further investigation of the roles of Fzd3 in psychoses to examine the genetic association of the *FZD3* gene with other types of psychoses, e.g., cocaine-induced paranoia or delusional type of bipolar disorders.

Conclusion

We examined genetic association of *FZD3* and found that two kinds of *FZD3* haplotypes showed strong associations with methamphetamine psychosis. Having the G-A-T-G or A-G-C-A haplotype of rs2241802-rs2323019-rs352203-rs880481 was a potent negative risk factor (odds ratios were 0.13 (95%CI; 0.07–0.22) and 0.086 (0.03–0.24), respectively) for methamphetamine psychosis. Our present and previous findings indicate that genetic variants of the *FZD3* gene affect susceptibility to two analogous but distinct dopamine-related psychoses, endogenous and substance-induced psychosis.

Competing interests

The authors declare that they have no competing interests.

Authors' contributions

HU conceived of the study, reviewed the manuscript and supervised all management, analysis, and interpretation of the data. MKi, YO, TK supervised by MT and MKo, genotyped samples and analyzed data, and MKi drafted manuscript and produced all tables. HU organized collaboration of Japanese substance abuse group, and HU, TI, MY, NU, NI, IS and NO collected genome samples and informed consents. HU and SK managed research expense. All authors read and approved for final manuscript.

Acknowledgements

We thank the Zikei Institute of Psychiatry (Okayama, Japan) and the Ministry of Health, Labor, and Welfare of Japan.

References

1. Bloom FE: **Advancing a neurodevelopmental origin for schizophrenia.** *Arch Gen Psychiatry* 1993, **50:**224-227.
2. Weinberger DR: **Implications of normal brain development for the pathogenesis of schizophrenia.** *Arch Gen Psychiatry* 1987, **44:**660-669.
3. Nusse R, Varmus HE: **Wnt genes.** *Cell* 1992, **69:**1073-1087.
4. Parr BA, McMahon AP: **Wnt genes and vertebrate development.** *Curr Opin Genet Dev* 1994, **4:**523-528.
5. Grove EA, Tole S, Limon J, Yip L, Ragsdale CW: **The hem of the embryonic cerebral cortex is defined by the expression of multiple Wnt genes and is compromised in Gli3-deficient mice.** *Development* 1998, **125:**2315-2325.
6. Hall AC, Lucas FR, Salinas PC: **Axonal remodeling and synaptic differentiation in the cerebellum is regulated by WNT-7a signaling.** *Cell* 2000, **100:**525-535.
7. Lucas FR, Salinas PC: **WNT-7a induces axonal remodeling and increases synapsin I levels in cerebellar neurons.** *Dev Biol* 1997, **192:**31-44.
8. Cotter D, Kerwin R, al-Sarraji S, Brion JP, Chadwich A, Lovestone S, Anderton B, Everall I: **Abnormalities of Wnt signalling in schizophrenia–evidence for neurodevelopmental abnormality.** *Neuroreport* 1998, **9:**1379-1383.
9. McMahon AP, Bradley A: **The Wnt-1 (int-1) proto-oncogene is required for development of a large region of the mouse brain.** *Cell* 1990, **62:**1073-1085.
10. Wang Y, Thekdi N, Smallwood PM, Macke JP, Nathans J: **Frizzled-3 is required for the development of major fiber tracts in the rostral CNS.** *J Neurosci* 2002, **22:**8563-8573.
11. Diwadkar VA, DeBellis MD, Sweeney JA, Pettegrew JW, Keshavan MS: **Abnormalities in MRI-measured signal intensity in the corpus callosum in schizophrenia.** *Schizophr Res* 2004, **67:**277-282.
12. Ananth H, Popescu I, Critchley HD, Good CD, Frackowiak RS, Dolan RJ: **Cortical and subcortical gray matter abnormalities in schizophrenia determined through structural magnetic resonance imaging with optimized volumetric voxel-based morphometry.** *Am J Psychiatry* 2002, **159:**1497-1505.
13. Kozlovsky N, Belmaker RH, Agam G: **GSK-3 and the neurodevelopmental hypothesis of schizophrenia.** *Eur Neuropsychopharmacol* 2002, **12:**13-25.
14. Katsu T, Ujike H, Nakano T, Tanaka Y, Nomura A, Nakata K, Takaki M, Sakai A, Uchida N, Imamura T, Kuroda S: **The human frizzled-3 (FZD3) gene on chromosome 8p21, a receptor gene for Wnt ligands, is associated with the susceptibility to schizophrenia.** *Neurosci Lett* 2003, **353:**53-56.
15. Yang J, Si T, Ling Y, Ruan Y, Han Y, Wang X, Zhang H, Kong Q, Li X, Liu C, Zhang D, Zhou M, Yu Y, Liu S, Shu L, Ma D, Wei J: **Association study of the human FZD3 locus with schizophrenia.** *Biol Psychiatry* 2003, **54:**1298-1301.
16. Zhang Y, Yu X, Yuan Y, Ling Y, Ruan Y, Si T, Lu T, Wu S, Gong X, Zhu Z, Yang J, Wang F, Zhang D: **Positive association of the human frizzled 3 (FZD3) gene haplotype with schizophrenia in Chinese Han population.** *Am J Med Genet B Neuropsychiatr Genet* 2004, **129B(1):**16-19.
17. Hashimoto R, Suzuki T, Iwata N, Yamanouchi Y, Kitajima T, Kosuga A, Tatsumi M, Ozaki N, Kamijima K, Kunugi H: **Association study of the frizzled-3 (FZD3) gene with schizophrenia and mood disorders.** *J Neural Transm* 2005, **112:**303-307.
18. Ide M, Muratake T, Yamada K, Iwayama-Shigeno Y, Iwamoto K, Takao H, Toyota T, Kaneko N, Minabe Y, Nakamura K, Kato T, Mori N, Asada T, Someya T, Yoshikawa T: **Genetic and expression analyses of FZD3 in schizophrenia.** *Biol Psychiatry* 2004, **56:**462-465.
19. Wei J, Hemmings GP: **Lack of a genetic association between the frizzled-3 gene and schizophrenia in a British population.** *Neurosci Lett* 2004, **366:**336-338.
20. Sato M: **A lasting vulnerability to psychosis in patients with previous methamphetamine psychosis.** *Ann N Y Acad Sci* 1992, **654:**160-170.
21. Ujike H, Sato M: **Clinical features of sensitization to methamphetamine observed in patients with methamphetamine dependence and psychosis.** *Ann N Y Acad Sci* 2004, **1025:**279-287.
22. Snyder SH: **Amphetamine psychosis: a "model" schizophrenia mediated by catecholamines.** *Am J Psychiatry* 1973, **130:**61-67.
23. Ujike H: **Stimulant-induced psychosis and schizophrenia: the role of sensitization.** *Curr Psychiatry Rep* 2002, **4:**177-184.
24. Kazahaya Y, Akimoto K, Otsuki S: **Subchronic methamphetamine treatment enhances methamphetamine- or cocaine-induced dopamine efflux in vivo.** *Biol Psychiatry* 1989, **25:**903-912.
25. Laruelle M, Abi-Dargham A, van Dyck CH, Gil R, D'Souza CD, Erdos J, McCance E, Rosenblatt W, Fingado C, Zoghbi SS, Baldwin RM, Seibyl JP, Krystal JH, Charney DS, Innis RB: **Single photon emission computerized tomography imaging of amphetamine-induced dopamine release in drug-free schizophrenic subjects.** *Proc Natl Acad Sci USA* 1996, **93:**9235-9240.
26. Prakash N, Brodski C, Naserke T, Puelles E, Gogoi R, Hall A, Panhuysen M, Echevarria D, Sussel L, Weisenhorn DM, Martinez S, Arenas E, Simeone A, Wurst W: **A Wnt1-regulated genetic network controls the identity and fate of midbrain-dopaminergic progenitors in vivo.** *Development* 2006, **133:**89-98.

27. Panhuysen M, Vogt Weisenhorn DM, Blanquet V, Brodski C, Heinzmann U, Beisker W, Wurst W: **Effects of Wntl signaling on proliferation in the developing mid-/hindbrain region.** *Mol Cell Neurosci* 2004, **26:**101-111.
28. Lovestone S, Killick R, Di Forti M, Murray R: **Schizophrenia as a GSK-3 dysregulation disorder.** *Trends Neurosci* 2007, **30:**142-149.
29. Bibb JA: **Decoding dopamine signaling.** *Cell* 2005, **122:**153-155.
30. Emamian ES, Hall D, Birnbaum MJ, Karayiorgou M, Gogos JA: **Convergent evidence for impaired AKT1-GSK3beta signaling in schizophrenia.** *Nat Genet* 2004, **36:**131-137.
31. Beasley C, Cotter D, Khan N, Pollard C, Sheppard P, Varndell I, Lovestone S, Anderton B, Everall I: **Glycogen synthase kinase-3beta immunoreactivity is reduced in the prefrontal cortex in schizophrenia.** *Neurosci Lett* 2001, **302:**117-120.
32. Yang SD, Yu JS, Lee TT, Yang CC, Ni MH, Yang YY: **Dysfunction of protein kinase FA/GSK-3 alpha in lymphocytes of patients with schizophrenic disorder.** *J Cell Biochem* 1995, **59:**108-116.
33. Nadri C, Kozlovsky N, Agam G, Bersudsky Y: **GSK-3 parameters in lymphocytes of schizophrenic patients.** *Psychiatry Res* 2002, **112:**51-57.
34. Proitsi P, Li T, Hamilton G, Di Forti M, Collier D, Killick R, Chen R, Sham P, Murray R, Powell J, Lovestone S: **Positional pathway screen of wnt signaling genes in schizophrenia: association with DKK4.** *Biol Psychiatry* 2008, **63:**13-16.
35. Svenningsson P, Tzavara ET, Carruthers R, Rachleff I, Wattler S, Nehls M, McKinzie DL, Fienberg AA, Nomikos GG, Greengard P: **Diverse psychotomimetics act through a common signaling pathway.** *Science* 2003, **302:**1412-1415.
36. Beaulieu JM, Sotnikova TD, Yao WD, Kockeritz L, Woodgett JR, Gainetdinov RR, Caron MG: **Lithium antagonizes dopamine-dependent behaviors mediated by an AKT/glycogen synthase kinase 3 signaling cascade.** *Proc Natl Acad Sci USA* 2004, **101:**5099-5104.
37. Kozlovsky N, Amar S, Belmaker RH, Agam G: **Psychotropic drugs affect Ser9-phosphorylated GSK-3 beta protein levels in rodent frontal cortex.** *Int J Neuropsychopharmacol* 2006, **9:**337-342.
38. Alimohamad H, Sutton L, Mouyal J, Rajakumar N, Rushlow WJ: **The effects of antipsychotics on beta-catenin, glycogen synthase kinase-3 and dishevelled in the ventral midbrain of rats.** *J Neurochem* 2005, **95:**513-525.

Biochemical and Biophysical Research Communications 374 (2008) 737–741

Contents lists available at ScienceDirect

Biochemical and Biophysical Research Communications

journal homepage: www.elsevier.com/locate/ybbrc

Ubiquitin ligase Kf-1 is involved in the endoplasmic reticulum-associated degradation pathway

Yoshiaki Maruyama, Misa Yamada, Kou Takahashi, Mitsuhiko Yamada *

Department of Psychogeriatrics, National Institute of Mental Health, National Center of Neurology and Psychiatry, 4-1-1 Ogawahigashi, Kodaira, Tokyo 187-8553, Japan

ARTICLE INFO

Article history:
Received 18 July 2008
Available online 31 July 2008

Keywords:
Kf-1
RNF103
RING finger
E3 ubiquitin ligase
Proteasome
ERAD
Derlin-1
VCP

ABSTRACT

Kf-1 was first identified as a gene showing enhanced expression in the cerebral cortex of a sporadic Alzheimer's disease patient. To date, however, the functional properties of Kf-1 protein remain unknown. In this study, immunohistochemical analysis showed that Kf-1 immunoreactivity was detected in rat hippocampus and cerebral cortex neurons. Interestingly, it was colocalized with endoplasmic reticulum (ER) marker. To investigate the specific function of Kf-1 protein, we generated Myc tagged wild type Kf-1 (Myc-Kf-1WT) and RING finger domain deletion mutant of Kf-1 (Myc-Kf-1ΔR), and then transfected in HEK293 cells. Myc-Kf-1WT displayed a reticular pattern typical of ER localization, with large perinuclear aggregates and colocalized with ER marker, calnexin. Myc-Kf-1WT facilitated ubiquitination of endogenous proteins, whereas Myc-Kf-1ΔR did not show ubiquitin ligase activity. In addition, we found that Kf-1 interacted with components of the ER-associated degradation (ERAD) pathway, including Derlin-1 and VCP. Taken together, these properties suggest that Kf-1 is an ER ubiquitin ligase involved in the ERAD pathway.

Kf-1, also called RING finger protein 103 (RNF103), was originally cloned as the gene whose expression was augmented in the cerebral cortex of a sporadic Alzheimer's disease patient [1]. We previously reported that *kf-1* gene expression is significantly increased in rat hippocampus and frontal cortex after chronic treatment with antidepressants [2]; after physiological therapy for depression, such as repeated electroconvulsive treatment [3]; and after repetitive transcranial magnetic stimulation [4]. Kf-1 is highly conserved among human, mouse, and rat, and is widely expressed in many different organs, including brain, heart, kidney, spleen, and lung [1–3]. Thus, Kf-1 is an interesting protein involved in brain function as well as general housekeeping functions of the cell. To date, however, the functional properties of Kf-1 protein remain unknown.

Kf-1 contains several hydrophobic regions at its N-terminal and middle regions, suggesting that Kf-1 is a membrane sorting protein [1,2]. Moreover, Kf-1 contains a C-terminal C3H2C3 RING finger domain that consists of a double-ring structure containing six cysteine and two histidine residues, coordinating two zinc ions [1,2]. The RING-finger-containing C terminus of Kf-1 has been shown to activate ubiquitin-conjugating enzyme (E2)-dependent ubiquitination *in vitro*, indicating that Kf-1 acts as an E3 ubiquitin ligase [5]. Integral membrane E3 ubiquitin ligases containing C3H2C3 RING fingers, such as HRD1 [6] and autocrine motility factor receptor (gp78/AMFR) [7,8], have been identified in mammals. These E3 ubiquitin ligases are located in endoplasmic reticulum (ER) and are involved in ER-associated degradation (ERAD). ERAD is a protein quality control mechanism that eliminates misfolded secretory and integral membrane proteins from ER through an ubiquitin-dependent proteasomal degradation pathway [9–11].

Although the machinery driving ERAD remains largely unknown, it does involve several different proteins at each step [11]. The process begins with the recognition of a misfolded protein substrate, likely involving certain chaperones. Next, the substrate is transported across the ER membrane through a protein-conducting channel. In mammals, an integral membrane protein, Derlin-1, has been identified as a protein-conducting channel that receives misfolded protein substrates from ER chaperones and transports these substrates [9]. Once substrates reach the cytosolic side of the membrane, most are polyubiquitylated by ubiquitin ligases. The polyubiquitin chain is subsequently recognized by a cytosolic ATPase valosin-containing protein (VCP) and its heterodimeric cofactors Ufd1 and Npl4. The hydrolysis of ATP presumably pulls the substrate into the cytosol, where it can be captured by proteasomes for degradation [12]. Previous studies indicate that Derlin-1 binds to VCP and its cofactors Ufd1 and Npl4 [9,13]. Moreover, ER-resident ubiquitin ligase HRD1, as well as gp78/AMFR, assembled within the Derlin-1/VCP complex to facilitate ubiquitination of the ERAD substrate [14].

On the basis of the structural features of Kf-1, we considered the possibility that Kf-1 may be a novel ER-resident ubiquitin ligase. In this study, we provide the first direct evidence that Kf-1 located in

* Corresponding author. Fax: +81 42 346 1994.
E-mail address: mitsu@ncnp.go.jp (M. Yamada).

0006-291X/$ - see front matter © 2008 Elsevier Inc. All rights reserved.
doi:10.1016/j.bbrc.2008.07.126

the ER and the C3H2C3 RING finger-containing C-terminal domain is essential for ubiquitin ligase activity. Our results also provide a link between Kf-1 and the Derlin-1/VCP complex. These properties suggest that Kf-1 is a C3H2C3 RING finger-containing ubiquitin ligase involved in the ERAD pathway.

Materials and methods

Construction of mammalian expression plasmids. Wild-type human Kf-1 (Kf-1WT) was generated with the following set of primers: 5′-GAA TTC AGA TGT GGC TGA AGC TT-3′ and 5′-CTC GAG GAC AAA TTG CAC ATG AAG-3′. These primers contain either EcoRI or XhoI restriction enzyme sites (underlined) to facilitate subcloning. The PCR product was subcloned into a pCR®-Blunt II-TOPO® vector. To construct a RING finger domain deletion mutant of Kf-1 (Kf-1ΔR), we digested the Kf-1WT-containing pCR®-Blunt II-TOPO® vector with NdeI to remove the RING finger domain of Kf-1 (Δ596–673). To fuse the Myc tags to the N termini of Kf-1WT and Kf-1ΔR, we digested both constructs with EcoRI/XhoI and cloned them into an EcoRI/XhoI-digested pCMV-Myc vector (Clontech, Mountain View, CA). An N-terminal hemagglutinin-tagged human ubiquitin (HA-Ub) was generated with the following set of primers: 5′-CCG GAA TTC GGA TGC AGA TCT TCG TGA AGA CT-3′ and 5′-CCG CTC GAG TCA CCC ACC TCT GAG ACG GA-3′. These primers contain either EcoRI or XhoI restriction enzyme sites (underlined) to facilitate subcloning. The ubiquitin construct was digested with EcoRI/XhoI and cloned into an EcoRI/XhoI-digested pCMV-HA vector (Clontech). After construction, the DNA sequences of all constructs were confirmed by DNA sequence analysis.

Animals. Eight-week-old male Sprague–Dawley rats were obtained from Clea Japan, Inc. (Tokyo, Japan). Animal care and use were in accordance with institutional guidelines.

Immunohistochemistry. Rats were anesthetized with sodium pentobarbital and transcardially perfused with 4% paraformaldehyde (Sigma) in 0.1 M phosphate buffer (pH 7.4). The brains were then cryoprotected and quickly frozen. The brain was sectioned (40 μm) using a cryostat HM550 (Microm, Germany). Sections were permeabilized for 20 min with 0.1% Triton X-100 (Sigma) at room temperature, and then blocked for 1 h with 1% fetal calf serum in phosphate-buffered saline (PBS). After washed with PBS, sections were exposed to each primary antibody in blocking buffer for overnight at 4 °C. The primary antibodies used were as follows: mouse monoclonal anti-NeuN antibody (1:500; Chemicon); mouse monoclonal anti-GFAP antibody (1:500; Chemicon); mouse monoclonal anti-KDEL antibody (1:200; Stressgen Bioreagents, Victoria, BC, Canada); and rabbit polyclonal anti-Kf-1 antibody (1:500; TransGenic Inc., Japan). After incubation with primary antibodies, cells were labeled for 1 h with Alexa Fluor®488-labeled anti-mouse IgG (H + L) or Alexa Fluor®633-labeled anti-rabbit IgG (H + L) (1:500; Invitrogen). Unbound secondary antibodies were washed out before visualization. Fluorescent microscopy was performed using a Fluoview FV1000 confocal microscope (Olympus, Tokyo, Japan).

Culture and transfection of HEK293 cells. Human embryonic kidney 293 (HEK293) cells were grown at 37 °C in a 5% CO_2 atmosphere in Dulbecco's modified Eagle's medium (Sigma, St. Louis, MO) containing 10% heat-inactivated fetal calf serum and antibiotics (Invitrogen, Carlsbad, CA). Cells grown in 35- or 100-mm plates to 50–80% confluence were transfected with expression plasmids using Lipofectamine 2000 (Invitrogen).

Immunocytochemistry. Twenty-four to forty-eight hours after transfection, immunocytochemistry was performed on HEK293 cells seeded onto poly-L-lysine-coated cover glasses. Cells were washed with PBS, fixed for 20 min with 4% paraformaldehyde, and permeabilized for 5 min with 0.1% Triton X-100 (Sigma) at room temperature. After washing with PBS, cells were blocked for 1 h with 1% bovine serum albumin (BSA)/PBS and then exposed to each primary antibody in 0.5% BSA/PBS for 2 h. The primary antibodies used were as follows: mouse monoclonal anti-Myc antibody (1:250; Clontech); rabbit polyclonal anti-HA antibody (1:100; Clontech); rabbit polyclonal anti-calnexin antibody (1:250; Stressgen Bioreagents, Victoria, BC, Canada); rabbit polyclonal anti-giantin antibody (1:250; Covance, Denver, PA); and rabbit polyclonal anti-prohibitin antibody (1:250; Abcam, Cambridge, MA). After incubation with primary antibodies, cells were labeled for 1 h with Alexa Fluor®488-labeled anti-mouse IgG (H + L) or Alexa Fluor®633-labeled anti-rabbit IgG (H + L) (1:500; Invitrogen). Unbound secondary antibodies were washed out before visualization. For nuclear staining, cells were labeled for 15 min with propidium iodide stain (1 μM; Invitrogen). For Brefeldin A (BFA) treatment, cells were incubated with 300 nM BFA (Calbiochem) or carrier (DMSO) for 18 h before use. Fluorescent microscopy was performed using a Fluoview FV1000 confocal microscope. For comparison, images were taken with laser power and gain held constant to allow direct comparison between cells.

Protein extract preparation, immunoblotting, and immunoprecipitation. Sixteen hours after transfection, cells were incubated with 10 μM MG132 (Sigma); 10 mM 3-methyladenine (3-MA; Sigma); 20 mM NH_4Cl (Wako, Tokyo, Japan); or carrier (DMSO or water) for 24 h. Cells were gently washed twice in ice cold PBS, scraped into 1 ml of extraction buffer containing 20 mM Tris–HCl (pH 7.5), 138 mM NaCl, 3 mM KCl, 1 mM EGTA, 2 mM EDTA, 5 μg/ml aprotinin, 5 μg/ml leupeptin, 5 μg/ml pepstatin A, 0.4 mM pefabloc SC, 1 mM DTT, and 1% Triton X-100, and incubated for 15 min on ice. The cell extracts were then centrifuged at 16,000g for 10 min, and the protein content of the supernatant assayed (BCA Protein Assay Reagent; Pierce Biotechnology, Rockford, IL). Proteins were separated by SDS–PAGE (7.5–15% gels), and then transferred onto 0.45-μm nitrocellulose membranes using standard techniques. The membranes were blocked with 5% non-fat dried milk (NFDM) in 0.1% Tween-20 PBS (PBST), labeled with primary antibodies in 1% NFDM PBST, and washed with PBST prior to labeling with horseradish peroxidase (HRP)-conjugated secondary antibodies at 1:10,000 (anti-mouse IgG (H + L) from American Qualex, San Clemente, CA; or anti-rabbit IgG (H + L) from Vector Laboratories Inc., Burlingame, CA). The primary antibodies used were as follows: mouse monoclonal anti-Myc antibody (1:1000; Clontech); mouse monoclonal anti-HA antibody (1:500; Roche); mouse monoclonal anti-β-actin antibody (1:4000; Sigma); rabbit polyclonal anti-Derlin-1 antibody (1:1000; Medical & Biological Laboratories Co., LTD, Nagoya, Japan); and rabbit polyclonal anti-VCP antibody (1:1000; Santa Cruz Biotechnology, Inc., Santa Cruz, CA). The immunoreactive bands were visualized with the ECL system and scanned with a FUJIFILM LAS-3000 mini (FUJIFILM, Japan). For the immunoprecipitation experiments, all reactions were performed while tumbling the cell extracts at 4 °C. HEK293 cell protein extracts were pre-cleared for 1 h with Protein G Sepharose CL-4B beads (GE Healthcare) and then incubated for 3 h with antibody. Antibody–protein complexes were captured by adding Protein G Sepharose and incubated overnight to facilitate binding. Immunoprecipitated complexes were eluted from the beads using SDS sample buffer prior to SDS–PAGE and immunoblotting.

Results

Kf-1 is an ER protein expressed in hippocampus and cerebral cortex neurons

Since Kf-1 is associated with a pathophysiology of Alzheimer's disease [1] or alleviation of depression [2–4], the expression of the Kf-1 protein was investigated in rat brain by immunohistochemistry. Using specific anti-Kf-1 antibody, Kf-1 appeared in the

pyramidal cell layer of the hippocampal region and located in the neuron-specific nuclear protein (NeuN)-positive neurons (Fig. 1A, first row). By contrast, Kf-1 immunoreactivity was not presented in the glial fibrillary acidic protein (GFAP)-positive astrocytes (Fig. 1A, second row). In additon, Kf-1 staining pattern was very similar to that obtained with the anti-KDEL antibody, which recognizes the ER molecular chaperones GRP78 (BiP) and GRP94, suggesting that Kf-1 mainly resides in the ER (Fig. 1A, bottom row). Similar distribution pattern were observed in cerebral cortex region (Fig. 1B). These results indicated that Kf-1 is an ER protein expressed in hippocampus and cerebral cortex neurons.

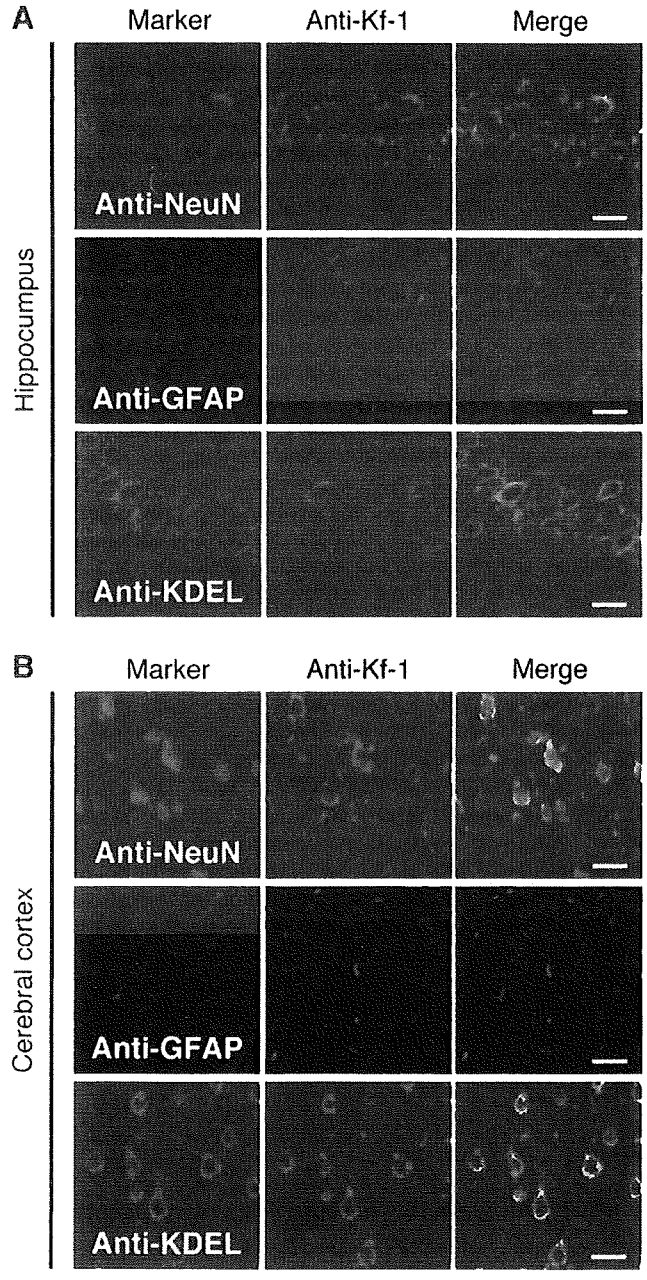

Fig. 1. Kf-1 is an ER protein expressed in hippocampus and cerebral cortex neurons. (A) Hippocumpus and (B) cerebral cortex. Brain slices were double stained with anti-Kf-1 antibody and a specific marker: anti-neuron-specific nuclear protein (NeuN, neuron), anti-glial fibrillary acidic protein antibody (GFAP, astrocyte) and anti-KDEL antibody (ER). Bar = 20 μm.

Kf-1 is an ER ubiquitin ligase

To investigate the specific function of Kf-1 protein, we generated Myc tagged wild type Kf-1 (Myc-Kf-1WT) and RING finger domain deletion mutant of Kf-1 (Myc-Kf-1ΔR), and then transfected in HEK293 cells. Note that HEK293 cells did not express any detectable endogenous Kf-1 protein (data not shown). As shown in Fig. 2A, Myc-Kf-1WT and Myc-Kf-1ΔR colocalized with calnexin (CNX), an integral ER membrane protein, and displayed a reticular pattern typical of ER localization. Occasionally, an accumulation of the Kf-1 as well as CNX was observed in Myc-Kf-1WT-expressing cells. We then overexpressed Myc-Kf-1WT or Myc-Kf-1ΔR with HA-Ub in HEK293 cells and the ubiquitin ligase activity of Kf-1 was analyzed by immunoblotting. Probing extracts from HA-Ub-expressing cells with anti-HA antibody detected slowly migrating smears of high molecular weight HA-Ub chains (Fig. 2B, first row). Cells expressing Myc-Kf-1WT showed increased accumulation of HA-Ub chains compared to cells transfected with empty plasmid and cells expressing Myc-Kf-1ΔR. This result indicated that Kf-1 facilitated ubiquitination of endogenous proteins. Taken together, these results indicated that the Kf-1 is an ubiquitin ligase located in ER. Interestingly, we probed the blots with anti-Myc

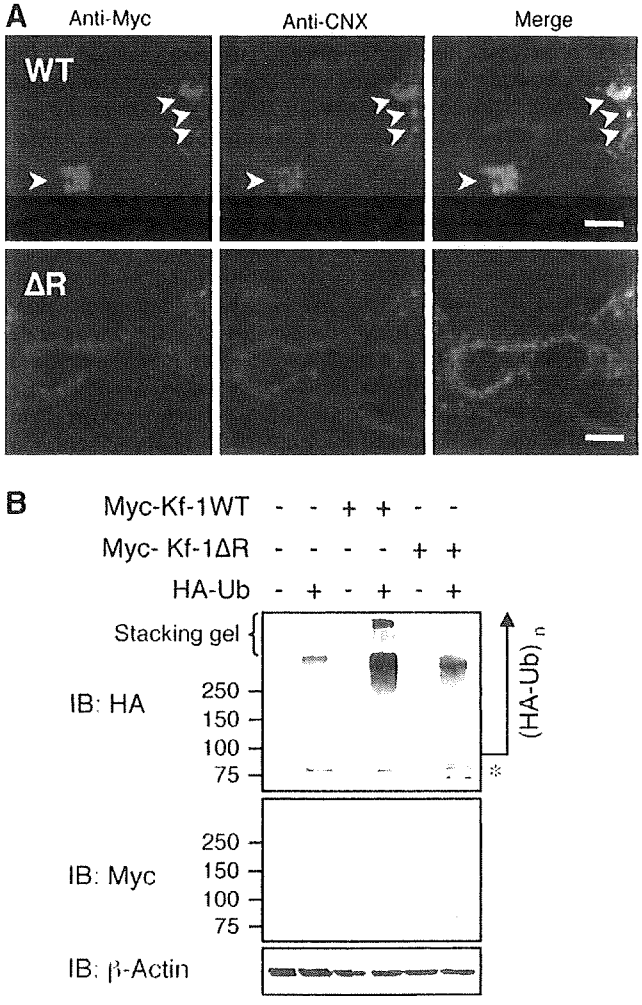

Fig. 2. Kf-1 is an ER ubiquitin ligase. (A) HEK293 cells expressing either Myc-Kf-1WT or Myc-Kf-1ΔR were double stained with antibodies against Myc tag and calnexin (CNX), an ER membrane protein. Myc-Kf-1WT accumulated and colocalized with CNX (arrow). Bar = 10 μm. (B) RING finger Myc-Kf-1WT or Myc-Kf-1ΔR was transiently expressed in HEK293 cells with HA-Ub. Cell extracts were resolved by SDS–PAGE, and proteins were detected by immunoblotting with antibodies against Myc, HA, or β-actin. Molecular masses are in kDa. The asterisk (*) indicates a non-specific band recognized by the anti-HA antibody.

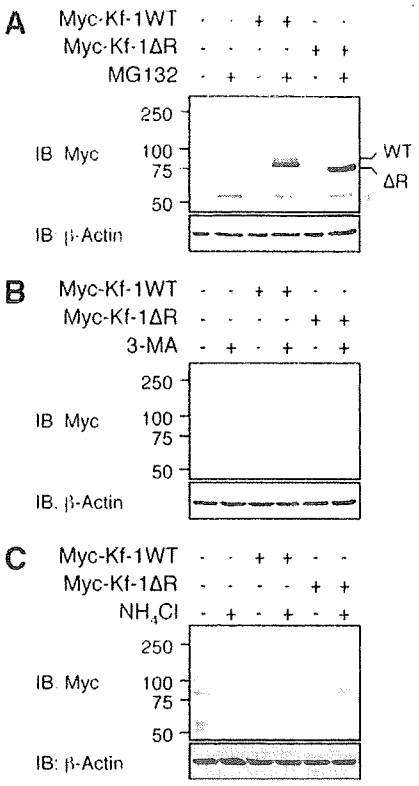

Fig. 3. Proteasomal degradation of Kf-1. Myc-Kf-1WT or Myc-Kf-1ΔR was transiently expressed in HEK293 cells. Cells were treated with 10 μM MG132 (A), 10 mM 3-MA (B), or 20 mM NH_4Cl (C) for 24 h. Cell extracts were resolved by SDS–PAGE, and proteins were detected by immunoblotting with antibodies against Myc or β-actin. Molecular masses are in kDa. The asterisk (*) indicates a non-specific band recognized by the anti-Myc antibody that was increased after treatment with MG132.

antibody for Myc-Kf-1WT or Myc-Kf-1ΔR protein; however, Myc-Kf-1 proteins were barely detected (Fig. 2B, second row).

Proteasomal degradation of Kf-1

A previous study showed that Dorfin (*do*uble *r*ing-*f*inger pro*tein*), another ubiquitin ligase, has only been detected in samples treated with a proteasome inhibitor [15]. Since most E3 ubiquitin ligases have autoubiquitinating activity and target themselves for proteasomal degradation, we investigated whether Kf-1 is degraded by the ubiquitin–proteasome system. Adding the proteasome inhibitor MG132 (10 μM, 24 h) to culture medium 16 h after transfection markedly increased the amounts of Myc-Kf-1WT and Myc-Kf-1ΔR, which could be detected easily on immunoblots (Fig. 3A). A single, dense ~80-kDa band from Myc-Kf-1WT samples and a 70-kDa band from Myc-Kf-1ΔR samples were detected along with slowly migrating smears possibly related to ubiquitinated Kf-1 proteins. Similar results were found with another specific proteasome inhibitor, epoxomicin (data not shown).

To investigate whether Kf-1 proteins were degraded by the autophagosomal/lysosomal pathway, we treated Myc-Kf-1WT- and Myc-Kf-1ΔR-expressing HEK293 cells with 3-MA, a macroautophagy inhibitor, or with NH_4Cl, a lysosomal proteolysis inhibitor. We found that neither 3-MA nor NH_4Cl increased the amount of Kf-1 proteins (Figs. 3B and C). These results indicated that Kf-1 is a short-lived protein specifically destroyed by the ubiquitin proteasome system.

Kf-1 Interacts with components of the ERAD pathway

To test whether Kf-1 interacts with the Derlin-1/VCP complex, HEK293 cells expressing either Myc-Kf-1WT or Myc-Kf-1ΔR with HA-Ub were solubilized and subjected to immunoprecipitation using anti-Myc antibody. In the immunoprecipitated samples, Myc-Kf-1WT- and Myc-Kf-1ΔR-immunoreactive proteins were detected as single, large bands along with slowly migrating smears (Fig. 4A, first row, right). In the input samples, however, Myc-Kf-1-immunoreactive proteins were hardly detected upon immunoblotting (Fig. 4A, first row, left). Note that for immunoblotting,

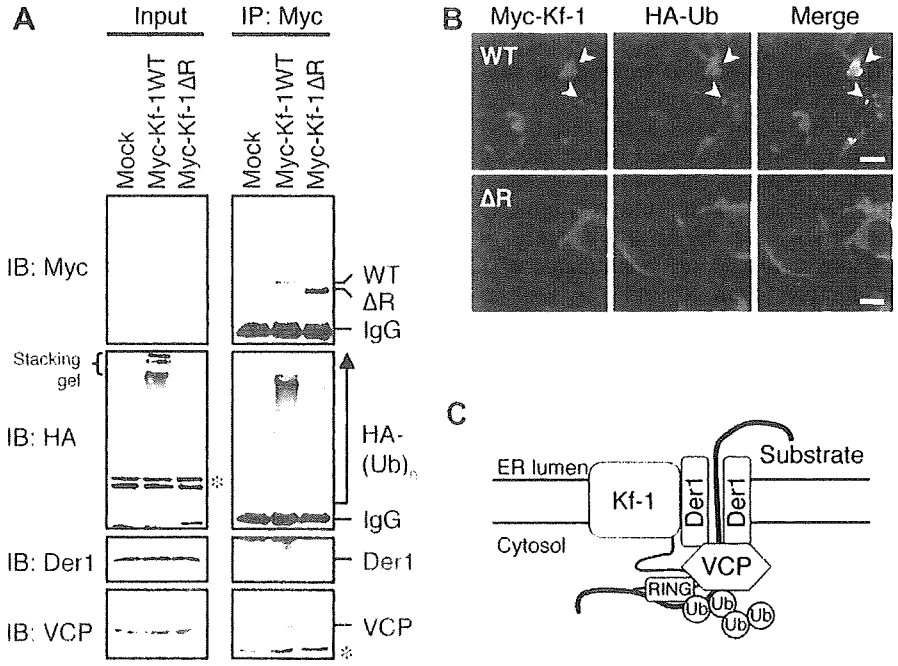

Fig. 4. Kf-1 interacts with components of the ERAD pathway. (A) Myc-Kf-1WT or Myc-Kf-1ΔR was transiently expressed in HEK293 cells with HA-Ub. Cell extracts were immunoprecipitated using anti-Myc antibody and then immunoblotted with antibodies against Myc, HA, Derlin-1, or VCP. For immunoblotting, 100 μg of cell extracts were used for input; for immunoprecipitation, 2.5 mg of cell extracts were used. The asterisk (*) indicates a non-specific band recognized by the anti-HA or anti-VCP antibodies. (B) Myc-Kf-1WT or Myc-Kf-1ΔR was transiently expressed in HEK293 cells with HA-Ub. Staining Kf-1 and ubiquitin with antibodies against their peptide tags revealed that ubiquitin also aggregates with Kf-1WT (arrow). Bar = 10 μm. (C) Scheme illustrating interactions between Kf-1, polyubiquitinated substrate, Derlin-1 and VCP.

100 μg of cell extracts were used as input, whereas for immunoprecipitation, 2.5 mg of cell extracts were used. In samples from cells expressing either Myc-Kf-1WT or Myc-Kf-1ΔR, treatment with anti-Myc antibody precipitated HA-Ub chains related to polyubiquitinated substrates and the Delin-1/VCP complex. These protein interactions were relatively lower in Myc-Kf-1ΔR-expressing cells than in Myc-Kf-1WT-expressing cells. We then determined whether Myc-Kf-1WT aggregates contained ubiquitin. Cells transiently expressing Myc-Kf-1WT or Myc-Kf-1ΔR with HA-Ub were double stained for their peptide tag and analyzed with fluorescence confocal microscopy. In cells expressing Myc-Kf-1WT, HA-Ub aggregated and colocalized with Myc-Kf-1WT (Fig. 4B, first row). By contrast, in cells expressing Myc-Kf-1ΔR, HA-Ub distributed throughout the cytoplasm and Myc-Kf-1ΔR displayed a reticular pattern typical of ER localization, without aggregates (Fig. 4B, bottom row). We conclude, therefore, that an ER ubiquitin ligase Kf-1 is involved in the ERAD pathway, where it facilitates the ubiquitination of ERAD substrates. (see scheme in Fig. 4C).

Discussion

In this study, we provide the first evidence that Kf-1 is a C3H2C3 RING finger-containing ubiquitin ligase involved in the ERAD pathway. In mammals, at least three ER-resident ubiquitin ligases, including gp78/AMFR, HRD1, and TEB4, are involved in the ERAD pathway. Kf-1 shares an interesting property with gp78/AMFR and HRD1, both of which contain several membrane spanning domains as well as a C3H2C3 RING finger domain in their C termini [6–8], in that these two ubiquitin ligases also interact with the Derlin-1/VCP complex. Kf-1 is a new member of ER-resident ubiquitin ligases that contribute to ERAD. Kf-1 also shares a property with HRD1, both proteins were located in the hippocampal and cerebral cortex regions [16]. Furthermore both proteins were detected in the NeuN-positive neurons, but not in the GFAP-positive astrocytes. Further studies will be required to investigate whether Kf-1 has specific brain function compared with other ER ubiquitin ligases involved in ERAD pathway.

We found here that Kf-1 proteins are degraded immediately by proteasomes. Although Kf-1 is a short-lived protein, it remains long enough to participate in the ubiquitination of endogenous substrates. Most ubiquitin ligases, including gp78/AMFR [8] and TEB4 [17], catalyze their own degradation in a RING finger- and proteasome-dependent manner. Thus, the ubiquitination activity of E3 ligases is essential for their stability. However, we observed that Kf-1ΔR is degraded as rapidly as Kf-1WT. Thus, it is unlikely that the ubiquitin ligase activity of Kf-1 affects Kf-1 stability. In addition, slowly migrating smears related to ubiquitinated Kf-1 proteins are observed in samples from Kf-1WT- as well as Kf-1ΔR-expressing cells after treatment with MG132 or immunoprecipitation. These observations suggested that Kf-1 may be potentially targeted for ubiquitination by other E3 ubiquitin ligases.

We focused on the interaction between Kf-1 and the Derlin-1/VCP complex, because this complex is known to involve in ERAD pathway. We showed that Kf-1 interacts with the Derlin-1/VCP complex. The interaction between Kf-1 and the Derlin-1/VCP complex is much smaller in Myc-Kf-1ΔR-expressing cells than in Myc-Kf-1WT-expresing cells. ERAD substrates have been proposed to be initially recognized by VCP; subsequently, the polyubiquitin chain is bound by both VCP and its cofactor Ufd1 and Npl4 [12]. This observation supports the view that the formation of the ERAD complex that includes Kf-1 depends on the ubiquitin ligase activity of Kf-1.

In conclusion, this report provides the first direct evidence that an ER-resident ubiquitin ligase, Kf-1, is involved in the ERAD pathway.

Acknowledgments

We thank Mr. Tomoyuki Nakagawa, Ms. Akiko Oku, and Dr. Kentaro Kudo for cloning the expression vectors. This work was supported by Grant-in-Aid for Young Scientists (B) (18790860) from The Ministry of Education, Culture, Sports, Science and Technology (MEXT), Japan.

References

[1] K. Yasojima, A. Tsujimura, T. Mizuno, Y. Shigeyoshi, J. Inazawa, R. Kikuno, K. Kuma, K. Ohkubo, Y. Hosokawa, Y. Ibata, T. Abe, T. Miyata, K. Matsubara, K. Nakajima, T. Hasimoto-Gotoh, Cloning of human and mouse cDNAs encoding novel zinc finger proteins expressed in cerebellum and hippocampus, Biochem. Biophys. Res. Commun. 231 (1997) 481–487.
[2] M. Yamada, M. Yamada, S. Yamazaki, K. Takahashi, G. Nishioka, K. Kudo, H. Ozawa, S. Yamada, Y. Kiuchi, K. Kamijima, T. Higuchi, K. Momose, Identification of a novel gene with RING-H2 finger motif induced after chronic antidepressant treatment in rat brain, Biochem. Biophys. Res. Commun. 278 (2000) 150–157.
[3] G. Nishioka, M. Yamada, K. Kudo, K. Takahashi, Y. Kiuchi, T. Higuchi, K. Momose, K. Kamijima, M. Yamada, Induction of kf-1 after repeated electroconvulsive treatment and chronic antidepressant treatment in rat frontal cortex and hippocampus, J. Neural. Transm. 110 (2003) 277–285.
[4] K. Kudo, M. Yamada, K. Takahashi, G. Nishioka, S. Tanaka, T. Hashiguchi, H. Fukuzako, M. Takigawa, T. Higuchi, K. Momose, K. Kamijima, M. Yamada, Repetitive transcranial magnetic stimulation induces kf-1 expression in the rat brain, Life Sci. 76 (2005) 2421–2429.
[5] K.L. Lorick, J.P. Jensen, S. Fang, A.M. Ong, S. Hatakeyama, A.M. Weissman, RING fingers mediate ubiquitin-conjugating enzyme (E2)-dependent ubiquitination, Proc. Natl. Acad. Sci. USA 96 (1999) 11364–11369.
[6] M. Kikkert, R. Doolman, M. Dai, R. Avner, G. Hassink, S. van Voorden, S. Thanedar, J. Roitelman, V. Chau, E. Wiertz, Human HRD1 is an E3 ubiquitin ligase involved in degradation of proteins from the endoplasmic reticulum, J. Biol. Chem. 279 (2004) 3525–3534.
[7] K. Shimizu, M. Tani, H. Watanabe, Y. Nagamachi, Y. Niinaka, T. Shiroishi, S. Ohwada, A. Raz, J. Yokota, The autocrine motility factor receptor gene encodes a novel type of seven transmembrane protein, FEBS Lett. 456 (1999) 295–300.
[8] S. Fang, M. Ferrone, C. Yang, J.P. Jensen, S. Tiwari, A.M. Weissman, The tumor autocrine motility factor receptor, gp78, is a ubiquitin protein ligase implicated in degradation from the endoplasmic reticulum, Proc. Natl. Acad. Sci. USA 98 (2001) 14422–14427.
[9] Y. Ye, Y. Shibata, C. Yun, D. Ron, T.A. Rapoport, A membrane protein complex mediates retro-translocation from the ER lumen into the cytosol, Nature 429 (2004) 841–847.
[10] B. Meusser, C. Hirsch, E. Jarosch, T. Sommer, ERAD: the long road to destruction, Nat. Cell Biol. 7 (2005) 766–772.
[11] P. Carvalho, V. Goder, T.A. Rapoport, Distinct ubiquitin-ligase complexes define convergent pathways for the degradation of ER proteins, Cell 126 (2006) 361–373.
[12] Y. Ye, H.H. Meyer, T.A. Rapoport, Function of the p97–Ufd1–Npl4 complex in retrotranslocation from the ER to the cytosol: dual recognition of nonubiquitinated polypeptide segments and polyubiquitin chains, J. Cell Biol. 162 (2003) 71–84.
[13] H.H. Meyer, Y. Wang, G. Warren, Direct binding of ubiquitin conjugates by the mammalian p97 adaptor complexes, p47 and Ufd1–Npl4, EMBO J. 21 (2002) 5645–5652.
[14] Y. Ye, Y. Shibata, M. Kikkert, S. van Voorden, E. Wiertz, T.A. Rapoport, Inaugural article: recruitment of the p97 ATPase and ubiquitin ligases to the site of retrotranslocation at the endoplasmic reticulum membrane, Proc. Natl. Acad. Sci. USA 102 (2005) 14132–14138.
[15] J. Niwa, S. Ishigaki, M. Doyu, T. Suzuki, K. Tanaka, G. Sobue, A novel centrosomal ring-finger protein, dorfin, mediates ubiquitin ligase activity, Biochem. Biophys. Res. Commun. 281 (2001) 706–713.
[16] T. Omura, M. Kaneko, N. Tabei, Y. Okuma, Y. Nomura, Immunohistochemical localization of a ubiquitin ligase HRD1 in murine brain, J. Neurosci. Res. 86 (2008) 1577–1587.
[17] G. Hassink, M. Kikkert, S. van Voorden, S.J. Lee, R. Spaapen, T. van Laar, E. Bartee, K. Früh, V. Chau, E. Wiertz, TEB4 is a C4HC3 RING finger-containing ubiquitin ligase of the endoplasmic reticulum, Biochem. J. 388 (2005) 647–655.

Journal of Neurochemistry JNC

JOURNAL OF NEUROCHEMISTRY | 2008 | 106 | 2375–2384 doi: 10.1111/j.1471-4159.2008.05579.x

Prg1 is regulated by the basic helix-loop-helix transcription factor Math2

Misa Yamada,* Yoshiko Shida,*,† Kou Takahashi,* Toshihiro Tanioka,† Yasuko Nakano,† Takashi Tobe‡ and Mitsuhiko Yamada*

*Department of Psychogeriatrics, National Institute of Mental Health, National Center of Neurology and Psychiatry, Tokyo, Japan

†Department of Pharmacogenomics, School of Pharmaceutical Science, Showa University, Tokyo, Japan

‡Center of Pharmaceutical Education, School of Pharmaceutical Science, Showa University, Tokyo, Japan

Abstract

Math2 (NEX-1/NeuroD6) is a member of the basic helix-loop-helix transcription factor family and is involved in neuronal differentiation and maturation. In this study, we identified the genes targeted by Math2 using DNA microarrays and cultured rat cortical cells transfected with Math2. Of the genes regulated by Math2, we focused on plasticity-related gene 1 (Prg1). Prg1 expression induced by Math2 was confirmed in cultured rat cortical cells and PC12 cells analyzed by real-time quantitative PCR. In the promoter region of rat Prg1, we identified four E-boxes [designated –E1 to –E4 (CANNTG)] recognized by the basic helix-loop-helix transcription factor. Using chromatin immunoprecipitation assays, we found that Math2 directly bound to at least one of these E-boxes. The Prg1 reporter assay showed that –E1 was critical for the regulation of Math2-mediated Prg1 expression. Investigation of the functional roles of Math2 and Prg1 in PC12 cells revealed that 72 h after transfection with either Math2 or Prg1, neurite length and number were significantly induced. Co-transfection with Prg1-siRNA completely inhibited Math2-mediated morphological changes. Our results suggest that Math2 directly regulates Prg1 expression and that the Math2–Prg1 cascade plays an important role in neurite outgrowth in PC12 cells.

Keywords: GeneChip®, Math2, neuronal plasticity, plasticity-related gene 1.

J. Neurochem. (2008) **106**, 2375–2384.

The basic helix-loop-helix (bHLH) transcription factors are implicated in the regulation of neuronal determination and differentiation in a wide variety of cell types. Genes for several mammalian bHLH transcription factors expressed in the developing nervous system have been isolated (Johnson *et al.* 1990; Akazawa *et al.* 1992; Duncan *et al.* 1992; Sasai *et al.* 1992; Feder *et al.* 1993; Ishibashi *et al.* 1993; Neuman *et al.* 1993; Sakagami *et al.* 1994; Takebayashi *et al.* 1995). Mammalian bHLH genes have been classified into two groups based on sequence homology, temporal expression pattern, and loss of function (Kageyama *et al.* 1997; Lee 1997). The first group, which includes Mash1, Math1, Neurogenin-1 (NeuroD3), and Neurogenin-2 (Math4A), are termed neuronal determination factors. These factors are, for the most part, expressed during early neurogenesis in proliferative neural progenitors. There are, however, some exceptions. The target disruption of these genes in mice leads to the loss of formation of neurons from neural precursors and results in the disruption of neuronal versus glial fate determination (Tomita *et al.* 2000; Nieto *et al.* 2001; Sun *et al.* 2001). The second group, which includes the NeuroD subfamily members, NeuroD, neuro D-related factor (NDRF)/NeuroD2, and Math2 (Nex1/NeuroD6), is referred to as neuronal differentiation factors. The studies of these genes, including those involving mutant mice, revealed that neural precursor cells fail to attain cell cycle arrest and to achieve the mature neuronal phenotype (Lee 1997; Farah *et al.* 2000; Schwab *et al.* 2000). Embryonic expression of NeuroD subfamily members is in general enriched in the subventricular zone, intermediate zone, and

Received April 7, 2008; revised manuscript received June 27, 2008; accepted July 10, 2008.

Address correspondence and reprint requests to Mitsuhiko Yamada, MD PhD., Department of Psychogeriatrics, National Institute of Mental Health, National Center of Neurology and Psychiatry, 4-1-1 Ogawahigashimachi, Kodaira, Tokyo 187-8553, Japan.
E-mail: mitsu@ncnp.go.jp

Abbreviations used: bHLH, basic helix-loop-helix; ChIP, chromatin immunoprecipitation; GO, gene ontology; HEK293, human embryonic kidney cells; LNGFR, low-affinity nerve growth factor receptor; LPA, lysophosphatidic acid; Prg1, plasticity-related gene 1; SDS, sodium dodecyl sulfate.

